



## Formation of the North Atlantic Craton: Timing and mechanisms constrained from Re–Os isotope and PGE data of peridotite xenoliths from S.W. Greenland

N. Wittig<sup>a,\*</sup>, M. Webb<sup>a</sup>, D.G. Pearson<sup>a</sup>, C.W. Dale<sup>a</sup>, C.J. Ottley<sup>a</sup>, M. Hutchison<sup>b</sup>, S.M. Jensen<sup>b,c</sup>, A. Luguet<sup>a,d</sup>

<sup>a</sup> Arthur Holmes Isotope Geology Laboratory, Department of Earth Sciences, Durham University, South Road, Durham, DH1 3LE, UK

<sup>b</sup> Geological Survey of Denmark and Greenland, Øster Voldgade 10, 1350 Copenhagen, K, Denmark

<sup>c</sup> Intex Resources ASA, Munkedamsveien 45A, PO 0250 Oslo, Norway

<sup>d</sup> Mineralogisch-Petrologisches Institut, Universität Bonn, Poppelsdorfer Schloss, 53115 Bonn, Germany

### ARTICLE INFO

#### Article history:

Received 24 November 2009

Received in revised form 7 June 2010

Accepted 11 June 2010

Editor: R.L. Rudnick

#### Keywords:

North Atlantic Craton

Nagssuqtoqidian mobile belt

Peridotite

Archean

Mantle melting

Platinum-group elements

Re–Os isotopes

### ABSTRACT

In this contribution we present platinum-group element (PGE) abundance and Os isotope data of North Atlantic Craton peridotite xenoliths ( $n=62$ ) sampled from four major clusters of kimberlite/ultramafic lamprophyre volcanism in W. Greenland. In addition, we analysed olivine separates from selected peridotites.

We find distinct differences in peridotites sampled from the northern (including the reworked Archean Nagssuqtoqidian mobile belt) and southern portions of the W. Greenland fragment of the NAC (WG–NAC). The heavily serpentinized harzburgitic to dunitic peridotites from the northern WG–NAC are typically marked by Os and Ir abundances that are somewhat lower than those of primitive mantle. Pt and Pd abundances are significantly depleted resulting in chondrite-normalized PGE patterns consistent with extensive melt extraction. As a consequence of the melting process, removal of sulphide and possibly a portion of residual PGE-rich alloys is likely. Typically, Os isotopes of these northern samples are unradiogenic ( $\gamma_{Os} = -14.2$  to  $-6.6$ , average ca.  $-9.2$ ), with separated olivines being similar in composition. The unradiogenic Os isotope compositions of the northern peridotites result in  $T_{RD}^{erupt}$  model ages clustering between 2.7 and 3.2 and also at ca. 2.0 Gyr. The grouping of the  $T_{RD}^{erupt}$  model ages correspond well with the U–Pb zircon ages derived from the trondjemite–tonalite–granodiorite continental crust ( $\sim 2.8$  Gyr) and the tectonic activity associated with the amalgamation and rifting of the WG–NAC and adjacent crust to the WG–NAC (Kangâmiut dykes  $\sim 2.0$  Gyr; Nagssuqtoqidian  $\sim 1.8$  Gyr). In detail however, a lack of Eoarchean Re depletion ages has to be recognized in this mantle root although the WG–NAC continental crust clearly preserves magmatic activity from the first 500 Ma of Earth's evolution. This lack of Eoarchean ages in the deep lithosphere may be due to unfortunate bias in the kimberlite eruption sites. Subordinate post-Archean melt extraction and metasomatic enrichment at ca. 2.0 Gyr is evident from the PGE and Os isotope systematics of some of these peridotites and is consistent with prolonged and episodic lithosphere evolution.

The southern WG–NAC peridotites appear to lack the extreme Pd depletion that is endemic in their northern counterparts. Generally the Os isotopes in these samples are more radiogenic ( $\gamma_{Os} = -11.5$  to  $+1.1$ , average ca.  $-7.2$ ) and show a very strong mode of 2.0 Gyr  $T_{RD}^{erupt}$  model ages. Only a small number of Archean  $T_{RD}^{erupt}$  model ages can be recognized in this sub-suite of the WG–NAC lithosphere. Despite their relatively depleted major element characteristics, the PGE systematics of the southern peridotites do not preserve evidence of mantle melting and Pd enrichment is evident in a number of samples. Olivine separates from selected southern peridotites typically yield older, Archean,  $T_{RD}^{erupt}$  model ages relative to the corresponding whole-rock peridotites, although Pd enrichment is evident in the olivine PGE patterns.

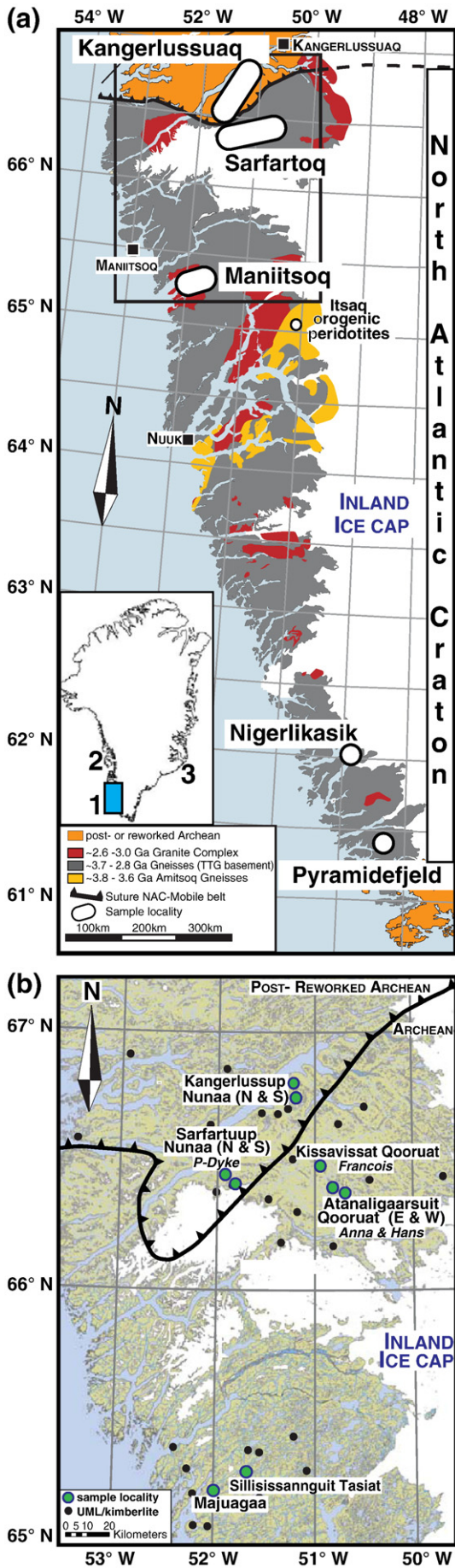
The majority of WG–NAC peridotite xenoliths with 2.7 to 3.1 Gyr and 2.0 Gyr  $T_{RD}^{erupt}$  model depletion ages have normal FeO abundances that are consistent with shallow mantle melting. A significant subset of peridotite xenoliths are enriched in FeO and have 2.3–2.6 Gyr  $T_{RD}^{erupt}$  model ages that do not align with specific, well-characterized magmatic events, although granulite-facies metamorphism has been proposed during this period. Pronounced PGE over-printing via metasomatism appears to have affected this set of peridotites.

Overall it is apparent that the WG–NAC mantle xenoliths record lithosphere stabilization at the Meso-Neoarchean boundary which was followed by selective modification that has altered and overprinted Os isotope, PGE systematics and FeO abundances in some parts of the lithosphere

© 2010 Elsevier B.V. All rights reserved.

\* Corresponding author. Department of Earth, Ocean, and Atmospheric Science & National High Magnetic Field Laboratory, Florida State University, 1800 E. Paul Dirac Drive, Tallahassee, FL 32310, United States. Fax: +1 850 644 0827.

E-mail addresses: [wittig@magnet.fsu.edu](mailto:wittig@magnet.fsu.edu), [hobbes@steinlaus.me.uk](mailto:hobbes@steinlaus.me.uk) (N. Wittig).



**1. Introduction**

The Archean portions of cratonic lithosphere are comprised predominantly of a trondjemite–tonalite–granodiorite (TTG) crustal lid with subordinate granites. This crustal skin is supported by a highly refractory and buoyant peridotitic root that may extend to depths of up to 250 km. In the process of studying Archean sub-continental lithospheric mantle (SCLM), the Slave and Kaapvaal cratons have been a focus of interest because they provide relatively abundant kimberlite-hosted mantle xenoliths, which allow large-scale investigation of Archean SCLM (Aulbach et al., 2004, 2007; Boyd, 1989; Boyd and Nixon, 1975; Irvine et al., 2001; 2003; Pearson et al., 1995; 2004; Walker et al., 1989). Consequently, insights from Slave and Kaapvaal Craton studies are often cited as blueprints for the depletion of the Earth’s mantle and the formation mechanism of Archean lithosphere, notwithstanding their substantially different geochemical composition. The different interpretation of these extreme compositions has, unsurprisingly, made the formation of Archean lithosphere a highly controversial issue (Aulbach et al., 2007; Bernstein et al., 2006a,b; Canil, 2004; Carlson et al., 2005; Griffin et al., 1999; Lee, 2006; Pearson and Wittig, 2008).

The West Greenlandic North Atlantic Craton (WG-NAC) hosts relatively abundant kimberlite/ultramafic lamprophyre pipes and sills (Andrews and Emeleus, 1975; Gaffney et al., 2007; Larsen, 1991a,b; Larsen and Rønso, 1993; Tachibana et al., 2006) that provide numerous mantle xenoliths (Fig. 1, Bernstein et al., 1998; Bernstein et al., 2006a,b; Bizzarro and Stevenson, 2003; Emeleus and Andrews, 1975; Wittig et al., 2008a). This SCLM appears to have escaped severe modal metasomatism and can be viewed as one of the more pristine records of Archean geodynamics (Bernstein et al., 2006b). As such it has been argued that the very refractory NAC peridotites from SW Greenland experienced shallow mantle depletion (>30%) in an Archean subduction zone (Wittig et al., 2008a).

The crustal lid of the WG-NAC has received substantially more attention than its mantle xenoliths and orogenic peridotites (e.g. Bennett et al., 2002; Friend et al., 2002) and has yielded some of the best-studied and well-dated examples of the Earth’s earliest magmatic crust and sediments (Caro et al., 2003; Frei and Rosing, 2001; Nutman et al., 2004 and references therein; Polat and Frei, 2005; Polat et al., 2002; 2003). A key question is the relationship of this crust to the underlying mantle. In order to establish a picture of the timing of WG-NAC SCLM formation, a radiogenic isotope system that fractionates during mantle melting and is robust against metasomatism is required. It has become clear that the Rb–Sr, Sm–Nd, U–Pb and Th–Pb isotope systems are exceedingly susceptible to the metasomatism that affects peridotites and in general they do not preserve age information concerning the initial depletion of SCLM (Pearson et al., 2003). The Lu–Hf isotope

**Fig. 1.** In panel (a) the North Atlantic Craton is shown in its present-day position relative to North America. Exposed Archean continental crust, the outline of well-defined cratons in addition to Pangaea and Proterozoic craton correlations (Bleeker, 2003) are outlined, whereas the dimensions of the WG-NAC and its exposed crust are highlighted in green. Note that the WG-NAC and the Disko Craton (Rae province) are shown as individual cratonic blocks separated by the Nagssugtoqidian mobile belt. Panel (b) shows a simplified tectonic map of the North Atlantic Craton in West Greenland (WG-NAC, A, 1 in inset). Note that xenolith localities from the Disko Craton (inset, “2”, Bernstein et al., 2006a) and East Greenland (inset, “3”, Bernstein et al., 1998) are given as well. The majority of the WG-NAC comprises TTG gneisses (grey). The Eoarchean Amitsoq gneisses are shown in yellow, whereas granitic portions are highlighted in red. The WG-NAC is sandwiched between post- or reworked Archean continental crust (orange). Xenoliths were collected from the kimberlite and UML (ultramafic lamprophyre) fields around Kangerlussuaq, Sarfartoq and Maniitsoq, which are located at the northern margin of the WG-NAC. Note that the Kangerlussuaq localities are situated in the reworked Archean region, although Os isotope data from these samples are typically very unradiogenic (see Fig. 6). The area at the northern margin of the WG-NAC is shown in greater detail in (c), where kimberlite/UML localities are given and xenolith sampling sites are highlighted. Kimberlite/UML sampling the continental mantle at Nigerlikasik and Pyramidefjeld are located at the southern margin of the WG-NAC.

system may hold the possibility of dating melt extraction if the targeted continental mantle has escaped depletion to extreme degrees (Wittig et al., 2006), which allows pyroxenes to remain in the residues of shallow mantle melting. Crucially, this mantle should be devoid of metasomatic enrichment due to interaction with silicate fluids in order to retain the initial depletion signature (e.g., Pearson and Nowell, 2004; Wittig et al., 2006, 2007). Emerging Lu–Hf isotope data, however, makes it clear that these conditions rarely exist in SCLM and that metasomatism is ubiquitous (Schmidberger et al., 2002; Shaw et al., 2007; Simon et al., 2007; Wittig et al., 2010a,b and references therein). In contrast, it has been demonstrated repeatedly that the siderophile Re–Os isotope system more faithfully records mantle depletion in the Archean than the afore mentioned lithophile isotope systems (e.g., Carlson et al., 2004; Chesley et al., 1999; Hanghøj et al., 2001; Irvine et al., 2003; Pearson et al., 2003; Pearson and Wittig, 2008) although its use in understanding post-Archean depletion of continental mantle appears to be problematic (e.g., Alard et al., 2002; Lorand et al., 2003; Wittig et al., 2010a; Rudnick and Walker, 2009).

Here we present platinum-group element (PGE) and Re–Os isotope data from WG-NAC peridotites, with a three-fold objective. Firstly, we attempt to determine the degree of mantle depletion by using siderophile trace element systematics in the WG-NAC peridotites and compare this with other estimates. This is a viable approach because lithophile major and trace elements are notoriously altered after initial melt depletion and it is difficult to constrain the extent of depletion, even in the refractory WG-NAC peridotites (Wittig et al., 2008a,b). Secondly, we attempt to resolve the timing of mantle depletion, lithosphere stabilization and later metasomatic alteration of the WG-NAC in order to document the extent of possible ancient SCLM beneath the WG-NAC. Our third objective is to map the likely extent of Archean lithospheric mantle beneath the reworked Archean crust that was deformed in the Proterozoic. This latter information is important in the context of on-going diamond exploration in this region (e.g., Hutchison and Frei, 2009).

## 2. Geological setting and samples

### 2.1. Crustal evolution of the Greenlandic North Atlantic Craton

The North Atlantic Craton (NAC, Fig. 1) outcrops in southern West Greenland, with minor exposure in the Nain Province (Canada) and within the Lewisian complex of N.W. Scotland (Bridgwater et al., 1973). This paper is only concerned with the mantle roots of the West Greenland portion of the NAC, hereafter abbreviated to WG-NAC. Within the WG-NAC, the northern region, Nuuk northwards, has received more academic attention than the area from Nuuk towards the southern margin of the NAC. This differential of intensity of study is due to a combination of diamond exploration and its accessibility by helicopter. The WG-NAC comprises several discrete trondjemite–tonalite–granodiorite terranes that appear to originate from Archean subduction zones (Steenfelt et al., 2005), although subordinate granites also occur. The crust later experienced episodes of granulite-facies metamorphism during amalgamation (Bridgwater et al., 1973).

The majority of the WG-NAC TTG crust formed between 2.8 and 3.0 Ga (Fig. 2a, e.g. Nutman et al., 2004). However, amongst those Meso-

to Neoproterozoic gneisses, U–Pb dating of zircon revealed a mosaic of substantially older terranes in the North (Aasivik terrane, ~3.7 Gyr, Rosing et al., 2001) and the centre of the WG-NAC (Isukasia [Amitsoq] and Tasiusarsuq terrane, ~3.8 and 3.9 Gyr, Fig. 2a) whereas supra-crustal rocks near Midternæs suggest sedimentation at ca. 3.6 Gyr (Nutman et al., 2004). Adjacent to the northern and southern margin of the WG-NAC, gneisses from the Nagssugtoquidian and the Ketilidian front were metamorphosed at ca. 1.8 Gyr and 1.2 Gyr (Fig. 2a). A brief and incomplete rifting episode of the WG-NAC emplaced the Kangâmiut dyke swarm at ca. 2 Ga, which is well-documented near Kangerlussuaq and Sarfartoq. Younger magmatism in southwest Greenland is associated with several incomplete rifting episodes emplacing major and minor alkaline and carbonatitic intrusives, including the Gardar pluton, during the Meso- and Neoproterozoic (ca. 1.4–1.2, ca. 0.55–0.61 Gyr; Tappe et al., 2007). The youngest magmatism occurred in the southern WG-NAC and comprises ultramafic lamprophyres (UML) and carbonatites (200–150 Ma; Tappe et al., 2007).

### 2.2. Xenolith-bearing magmatism

We provide data for xenoliths derived from kimberlite/UML clusters at the northern and southern margin of the WG-NAC (Fig. 1). The extent of the kimberlite/UML fields from around Kangerlussuaq and Sarfartoq spans the definable northern margin of the WG-NAC, sampled the SCLM both on- and off-craton in three episodes at ca. 556–568, 585–577 and 602–604 Ma (Heaman, 2005; Secher et al., 2009). The Kangerlussuaq localities are situated in the Nagssugtoquidian mobile belt close to the surface suture line that separates the pristine WG-NAC from Archean crust that has been extensively reworked (Fig. 1). The on-craton Sarfartoq kimberlite cluster is associated with the Sarfartoq alkaline province (Larsen, 1991a) and extends towards localities close to the Sukkertoppen ice cap (Garnet Lake). Some of these localities contain economic grades of diamonds (e.g. Hutchison and Frei, 2009; Jensen et al., 2003; 2004). A small number of samples are from the Maniitsoq kimberlite cluster, which is located closer to the centre of the WG-NAC and hosts eclogitic, wehrlitic and some lherzolitic xenoliths (Nielsen et al., 2008). Kimberlites from the southern margin of WG-NAC (Nigerlika-sik and Pyramidefjeld) are less voluminous and intruded as individual sills into the continental crust (TTG and granite) at approximately 164 Ma (Heaman, 2005; Secher et al., 2009), although carbonatitic and ultramafic lamprophyric magmatism appears to have been active between 150 and 200 Ma (Tappe et al., 2007).

### 2.3. Xenolith characteristics

The ultra-refractory dunite and harzburgite xenoliths from the northern portion of the WG-NAC have little constituent orthopyroxene, clinopyroxene and garnet (Table 1; Bizzarro and Stevenson, 2003; Wittig et al., 2008a). Similar xenolith compositions have been found on Ubekendt Ejland and in Southeast Greenland (Bernstein and Brooks, 1998; Bernstein et al., 1998, 2006a,b; Hanghøj et al., 2001). A sub-fraction of xenoliths from the northern WG-NAC are lherzolitic. Generally, serpentinization is substantial in the northern SCLM, and largely absent in the xenoliths from

**Fig. 2.** Relative probability plot of U–Pb ages (zircon) of continental crust from the WG-NAC (trondjemite–tonalite–granodiorite; TTG,  $n = 485$ ) and adjacent crust north and south of the craton margin (a) in comparison to  $T_{RD}^{RePt}$  model ages of northern and southern WG-NAC whole-rock peridotites (b, this study). Note the prominent peaks at 1.8–2.0 and between 2.8 and 3.2 Gyr in the whole-rock peridotite population that coincide with the magmatic production of the WG-NAC and adjacent crust as well as the emplacement of the Kangâmiut dykes (2.0 Gyr, green). For comparison, we also provide the associated histogram on which the density probability curve is based on. There does not appear to be a relevant relationship between the host volcanic rocks or the lamproites (light blue) with the derived  $T_{RD}$  ages from our peridotites. U/Pb data taken from literature (Nutman et al., 2004; Whitehouse et al., 1998). In (c) and (d) we compare  $Al_2O_3$  (wt.%) and FeO (wt.%) versus  $T_{RD}^{RePt}$  of northern and southern WG-NAC whole-rock peridotites. Note the low  $Al_2O_3$  abundance, highly variable FeO of the WG-NAC peridotites and the complete lack of correlation in  $Al_2O_3$ – $T_{RD}^{RePt}$  space (c). Also outlined are relevant geological events; (Kangâmiut Dykes [2.0 Gyr, green], granulite-facies metamorphism [2.3–2.6 Gyr] and lamproitite [light blue] and kimberlite magmatism [~0.17 omitted for clarity, ~0.6; 1.2–1.4 Gyr, red]). Samples with Archean and ~2 Gyr  $T_{RD}^{RePt}$  ages have FeO abundances consistent with shallow melt extraction (~2 GPa; 6 to 9 wt.%), whereas FeO enrichment (>9 wt.%) appears more common in samples with younger  $T_{RD}^{RePt}$  Os model ages that coincide with the magmatic activity in Labrador alkaline volcanic province and granulite-facies metamorphism. Olivine-whole-rock pairs are connected by tie lines and indicate that the olivines (diamonds) tend to yield ca. 2.8 Gyr  $T_{RD}^{RePt}$  model ages.

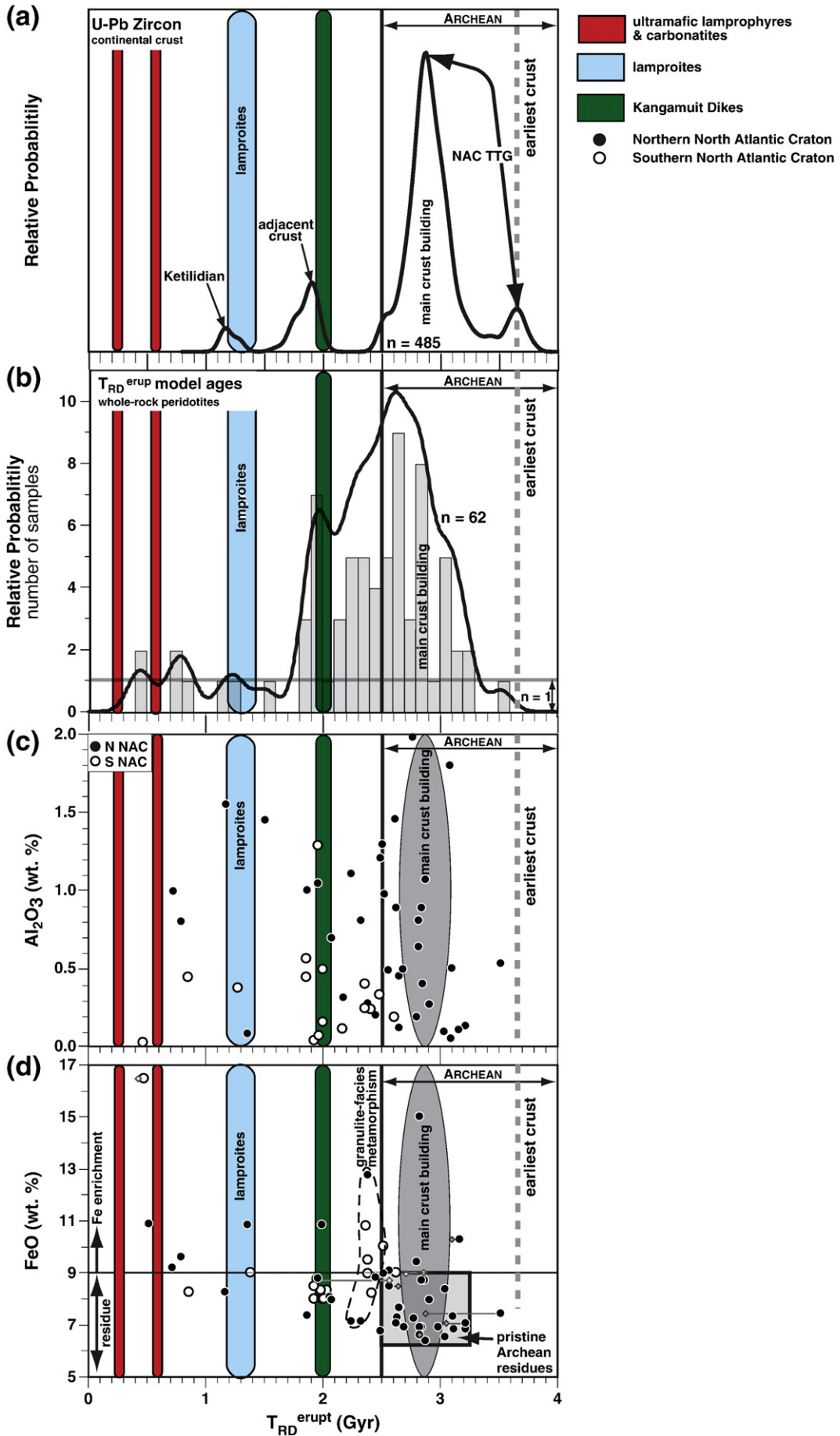


**Table 1**  
PGE and Re–Os isotope data of whole-rock peridotites from the northwestern margin North Atlantic Craton (on-craton) and adjacent Nagssuqtoqidian mobile belt (off-craton) (Greenland).

	474521	474527	464006	483806	477421	474535	474536	474537	474538	474541	474542	474543
Locality	Off-craton – North Kangerlussup Nunaa Kangerlussuaq				Off-craton – at craton margin Sarfartup Nunaa P-Dyke							
Latitude	66.770365				66.412516							
Longitude	– 51.195623				– 51.819434				– 51.463222			
<i>Modes (%)</i>												
ol	86.6	82.5	87.9	85.3	95.2	81.6	85.0	85.1	80.2	–	84.76	75.3
opx	10.6	10.9	5.4	8.7	0.0	12.3	6.0	9.6	8.7	–	5.4	12.1
cpx	2.7	0.81	6.7	3.0	4.8	0.5	7.4	0.0	2.4	–	1.0	0.1
spl	0.06	–	0.02	–	–	–	–	–	–	–	–	–
grt	–	5.84	–	2.98	–	5.61	1.61	5.32	8.74	–	8.83	12.49
<i>XRF (wt.%)</i>												
SiO <sub>2</sub>	42.07	42.44	41.92	42.71	41.03	40.51	41.67	42.65	42.46	–	42.19	42.85
TiO <sub>2</sub>	0.12	0.15	0.08	0.12	0.05	0.13	0.15	0.02	0.21	–	0.08	0.25
Al <sub>2</sub> O <sub>3</sub>	0.28	0.82	0.89	0.49	0.13	0.81	0.10	1.21	1.80	–	1.46	1.05
FeO*	7.96	7.14	7.29	8.50	7.66	9.60	6.54	6.78	8.38	–	7.08	8.80
MnO	0.11	0.11	0.11	0.08	0.16	0.13	0.10	0.12	0.13	–	0.12	0.14
MgO	48.13	46.93	48.80	46.76	48.88	47.29	49.67	48.23	45.39	–	47.49	45.08
CaO	0.68	0.54	0.37	0.81	1.27	0.84	1.11	0.18	0.93	–	0.76	0.79
Na <sub>2</sub> O	0.08	b.d.l.	b.d.l.	b.d.l.	b.d.l.	0.03	0.05	b.d.l.	0.09	–	b.d.l.	b.d.l.
K <sub>2</sub> O	0.10	0.05	0.02	0.04	0.41	0.05	0.04	0.06	0.05	–	0.04	0.06
P <sub>2</sub> O <sub>5</sub>	0.04	b.d.l.	b.d.l.	b.d.l.	0.01	0.03	0.04	b.d.l.	0.01	–	b.d.l.	b.d.l.
Total	99.56	101.38	99.48	99.52	99.61	99.43	99.47	100.38	99.45	–	98.98	99.90
LOI	12.28	2.68	12.43	11.26	2.51	11.82	10.84	12.62	11.55	–	11.25	10.96
<i>µg/g (ppm)</i>												
Zn	40.6	48.6	44.7	27.4	76.8	59.0	37.9	44.3	51.7	–	46.2	55.7
Cu	6.81	14.0	11.6	13.8	8.19	12.5	4.24	1.80	6.91	–	7.30	12.90
Ni	2160	2282	2274	2196	2298	2647	2586	2438	2288	–	2259	2056
Cr	1506	2336	2216	1916	1368	2221	1995	3201	2460	–	4059	3972
V	30.7	29.7	26.1	36.4	16.2	24.0	13.7	19.4	38.2	–	35.2	46.4
Ba	30.5	37.7	17.1	33.6	49.5	17.0	17.5	13.4	20.3	–	11.3	31.3
Sc	1.20	3.40	5.60	2.80	12.5	4.20	2.30	7.1	9.30	–	7.0	7.3
Co	111	112	97.5	102	106	122	101	103	101	–	95.20	102
Ga	0.547	0.80	0.968	1.13	1.35	0.78	0.49	0.253	1.38	–	0.871	1.63
Lu	0.004	0.010	0.013	0.012	0.015	0.014	0.003	0.011	0.020	–	0.016	0.014
Hf	0.161	0.135	0.093	0.182	0.371	0.130	0.221	0.053	0.170	–	0.109	0.218
<i>ng/g (ppb)</i>												
Os	1.04	4.29	3.56	4.48	3.41	0.86	2.01	3.28	2.45	2.99	3.49	2.17
Ir	1.14	4.06	3.49	5.17	1.11	0.66	1.73	3.04	2.42	3.08	3.35	2.83
Ru	1.49	7.96	6.63	10.62	5.63	2.34	2.65	4.05	4.88	7.89	6.56	4.39
Pt	0.60	3.16	3.59	4.40	0.50	0.59	1.73	0.13	1.67	1.37	4.07	9.97
Pd	0.18	1.73	1.96	2.44	0.10	1.44	0.09	0.16	0.26	0.50	0.13	0.99
Re	0.15	0.07	0.11	0.15	0.02	0.03	0.05	0.03	0.13	0.06	0.09	0.04
Total	PGE	4.46	21.20	19.23	27.11	10.76	5.90	8.22	10.66	11.67	15.83	17.60
Total	I-PGE	3.68	16.31	13.69	20.27	10.15	3.86	6.40	10.37	9.74	13.96	13.41
Total	P-PGE	0.78	4.89	5.55	6.84	0.60	2.04	1.82	0.29	1.92	1.87	4.20
<i>Chondrite-normalized</i>												
(Pt/Pd) <sub>N</sub>	1.80	1.00	1.00	0.98	2.67	0.22	10.15	0.44	3.50	1.49	17.67	5.50
(Os/Ir) <sub>N</sub>	0.85	0.98	0.95	0.80	2.85	1.22	1.08	1.00	0.94	0.90	0.97	0.71
(Pd/Ir) <sub>N</sub>	0.13	0.35	0.46	0.39	0.08	1.82	0.04	0.04	0.09	0.13	0.03	0.29
(Pt/Ir) <sub>N</sub>	0.24	0.35	0.46	0.38	0.20	0.41	0.45	0.02	0.31	0.20	0.55	1.59
(Ru/Ir) <sub>N</sub>	0.84	1.26	1.22	1.32	3.25	2.29	0.98	0.85	1.29	1.64	1.26	0.99
<sup>187</sup> Re/ <sup>188</sup> Os	0.699	0.083	0.150	0.158	0.025	0.175	0.117	0.049	0.216	0.103	0.126	0.078
<sup>187</sup> Os/ <sup>188</sup> Os	0.11407	0.11287	0.11114	0.11171	0.10977	0.12478	0.10780	0.11120	0.10860	0.10985	0.11098	0.11536
Γ Os	–8.3	–9.3	–10.7	–10.2	–11.8	0.3	–13.4	–10.6	–12.7	–11.7	–10.8	–7.3
<i>Os model ages (Myr)</i>												
T <sub>Ma</sub>	–3214	2745	3720	3711	2778	935	3951	2735	5485	3428	3469	2268
T <sub>RD</sub>	1990	2217	2435	2356	2620	552	2886	2426	2761	2610	2456	1858
T <sub>RD</sub> <sup>erupt</sup>	2911	2327	2632	2565	2653	789	3039	2490	3043	2746	2623	1961
<sup>187</sup> Os/ <sup>188</sup> Os <sub>initial</sub>	0.10762	0.11193	0.10968	0.11018	0.10953	0.12308	0.10666	0.11072	0.10663	0.10884	0.10975	0.11461

Modes, major and element composition taken from Wittig et al. (2008a). Model ages (Myr) are calculated after Walker et al. (1989) and Pearson et al. (1995). Chondrite is taken from McDonough and Sun (1995). <sup>187</sup>Os/<sup>188</sup>Os initial is calculated for an eruption age (580 Ma, Heaman, 2005). γOs after Meisel et al. (1996). Ru abundances were determined by ICP-MS using collision cell technology (Thermo-Scientific Xseries2).

Nigerlikasik and Pyramidefjeld. Thermobarometry on mantle xenoliths shows that the UML/kimberlite-host volcanic rocks sampled the SCLM over an interval of 180 km to depths of at least 220 km (Bizzarro and Stevenson, 2003; Sand et al., 2009). Only

minor phlogopite, calcite and apatite, assumed to have precipitated from the passing kimberlite-host, can be found in these xenoliths. Rare clinopyroxene and garnet from lherzolitic northern WG-NAC xenoliths have Hf–Nd isotope systematics identical to the

474544	474545	474546	474547	474551	474555	474557	474566	474573	474574	474575	474576	474577	P-dyke a	P-dyke b
92.8	81.0	82.9	81.0	83.8	78.0	89.3	79.4	87.7	85.5	82.2	95.4	71.6	84.2	79.7
1.5	13.3	9.8	13.9	4.5	15.9	9.1	13.5	8.2	10.2	10.8	0.0	21.1	5.9	5.8
2.7	1.3	4.2	0.01	7.4	2.3	1.6	2.9	3.6	1.4	1.1	1.0	2.2	4.1	10.3
-3.0	0	-	-	-	-	-	-	0.51	-	-	-	-	-	-
-	4.33	3.12	5.02	4.27	3.78	-	4.20	-	2.90	5.86	3.6	5.11	5.80	4.19
40.59	43.44	42.73	42.09	41.45	43.60	42.18	43.20	40.62	42.87	42.60	40.33	44.87	42.00	44.02
0.14	0.09	0.03	0.10	0.11	0.19	0.07	0.04	0.13	0.15	0.13	0.17	0.08	0.15	0.15
0.21	1.07	0.89	0.51	0.51	0.70	0.54	0.81	1.00	0.65	1.55	0.12	1.01	1.98	1.11
8.84	6.40	6.93	6.91	7.33	7.97	7.45	6.91	9.19	6.61	8.28	10.30	7.37	7.27	7.14
0.12	0.10	0.10	0.08	0.10	0.11	0.12	0.10	0.13	0.09	0.11	0.11	0.12	0.12	0.12
48.77	47.71	48.33	48.68	49.04	45.93	46.08	48.01	47.32	48.49	46.10	48.08	44.77	46.80	45.69
0.70	0.41	0.30	0.95	0.60	0.76	2.45	0.25	0.83	0.47	0.57	0.45	0.94	0.78	0.84
0.05	0.08	0.03	0.07	0.06	0.12	0.12	0.08	0.06	0.06	0.09	0.07	0.08	b.d.l	b.d.l
0.08	0.07	0.05	0.03	0.06	0.09	0.30	0.04	0.05	0.03	0.05	0.03	0.05	0.10	0.12
0.04	0.04	0.03	0.03	0.03	0.02	0.04	0.01	0.03	0.04	0.03	0.04	0.03	b.d.l	b.d.l
99.52	99.42	99.43	99.45	99.28	99.50	99.34	99.45	99.36	99.45	99.51	99.68	99.31	100.56	100.05
13.95	12.05	13.17	13.41	8.68	7.68	9.14	12.29	11.90	11.99	11.41	10.52	10.07	11.31	11.54
51.0	39.2	38.5	36.9	43.5	51.5	50.9	38.6	60.6	40.2	50.2	73.1	44.4	45.8	45.9
6.31	2.36	1.46	4.93	8.29	7.50	10.1	2.26	11.3	7.50	17.9	6.91	7.30	6.60	8.30
2475	2394	2496	2573	2523	2379	2252	2447	2643	2417	2210	2326	2229	2462	2284
1537	2511	2326	2046	3847	2050	3484	2242	2789	2244	1936	402	3749	4636	4004
18.6	20.2	19.9	17.7	23.8	47.0	73.7	18.5	27.5	21.5	30.4	19.8	36.9	41.40	41.30
18.8	16.8	8.70	10.7	22.8	25.6	42.1	12.3	12.4	11.6	14.8	20.2	19.7	33.0	46.3
b.d.l	7.40	5.50	2.20	7.70	3.80	4.50	5.70	6.30	4.10	7.00	b.d.l	8.70	9.90	6.90
106	98.2	93.7	101	96.1	96.7	99.3	100	119	96.0	100	119	99.44	97.36	92.86
0.648	0.28	0.22	0.30	0.59	1.11	1.59	0.23	0.92	0.700	0.86	0.383	0.65	0.963	0.968
0.003	0.011	0.007	0.006	0.007	0.013	0.008	0.008	0.015	0.007	0.021	0.004	0.007	0.016	0.011
0.138	0.081	0.058	0.131	0.154	0.162	0.824	0.068	0.139	0.202	0.160	0.114	0.139	0.191	0.183
1.26	2.88	3.06	5.02	0.96	2.67	0.89	6.09	1.55	4.80	3.00	0.96	1.95	5.16	4.21
1.04	2.64	3.16	3.82	0.80	3.23	0.80	4.76	3.37	4.61	3.03	0.98	2.70	4.61	2.88
-	3.79	6.07	1.64	1.23	4.83	2.26	7.33	-	3.19	8.56	1.18	8.12	7.57	10.86
1.08	0.04	0.36	4.11	0.03	1.72	0.27	0.12	3.37	0.87	2.47	0.07	2.78	0.83	1.45
0.50	0.02	0.01	0.02	0.05	0.45	0.07	0.09	2.10	0.05	5.38	0.01	0.36	0.51	0.03
0.05	0.02	0.02	0.06	0.04	0.11	0.29	0.03	0.04	0.01	0.05	0.04	0.04	0.04	0.07
20.35	-	9.37	12.65	14.61	3.07	12.89	4.30	18.39	-	13.52	22.44	3.21	15.90	18.69
9.39	-	9.31	12.29	10.48	2.99	10.73	3.96	18.18	-	12.60	14.59	3.12	12.77	17.35
10.96	1.59	0.06	0.37	4.14	0.08	2.16	0.34	0.21	5.46	0.92	7.85	0.09	3.14	1.34
1.17	0.93	28.01	107.21	0.40	2.09	2.08	0.79	0.87	9.45	0.25	3.25	4.21	0.88	25.66
1.12	1.01	0.90	1.22	1.12	0.77	1.03	1.19	0.43	0.97	0.92	0.91	0.67	1.04	1.36
0.40	0.01	0.002	0.005	0.05	0.11	0.07	0.01	0.52	0.01	1.47	0.01	0.11	0.09	0.01
0.47	0.01	0.05	0.49	0.02	0.24	0.15	0.01	0.45	0.09	0.37	0.03	0.46	0.08	0.23
-	0.92	1.23	0.27	0.99	0.96	1.81	0.99	-	0.44	1.81	0.77	1.93	1.05	2.42
0.189	0.031	0.031	0.053	0.177	0.198	1.565	0.025	0.126	0.015	0.136	0.222	0.108	0.035	0.078
0.11284	0.10817	0.10844	0.10978	0.10788	0.11588	0.11845	0.10851	0.12482	0.10842	0.12167	0.10788	0.11634	0.10899	0.11330
-9.3	-13.1	-12.8	-11.8	-13.3	-6.9	-4.8	-12.8	0.3	-12.9	-2.2	-13.3	-6.5	-12.4	-8.9
3920	3051	3018	2985	4845	3348	-552	2961	775	2899	1445	5872	2304	2966	2614
2202	2836	2800	2618	2876	1808	1460	2790	546	2802	987	2876	1723	2726	2141
2453	2876	2841	2688	3106	2071	3523	2823	717	2821	1170	3165	1868	2772	2244
0.11100	0.10787	0.10813	0.10927	0.10616	0.11380	0.10305	0.10827	0.12360	0.10828	0.12035	0.10572	0.11529	0.10865	0.11254

UML/kimberlite-host volcanic rocks, implying that these Al-bearing minerals originated from passing magmas at the time of UML/kimberlite emplacement (Wittig et al., 2008b). A detailed examination of major element systematics of the WG-NAC peridotites

can be found in Wittig et al. (2008a), who concluded that despite the highly refractory nature of these WG-NAC peridotites (e.g.,  $\text{Al}_2\text{O}_3 < 2$  wt.%, Fig. 2c), major element constraints are not suitable for the determination of parameters such as depths of melting.

**Table 2**

PGE and Re–Os isotope data of whole-rock peridotites from the southwestern margin of the North Atlantic Craton (Pyramidefjeld).

	G-06-7A	G-06-4A	G-06-4B	G-06-4C	G-06-4D	G-06-6A	G-06-6B	G-06-6C	G-06-7A	G-06-7B	G-06-7C	G-06-7D
Locality	On-craton—South Pyramidefjeld											
Latitude	61.424276											
Longitude	−48.277874											
<i>Modes (%)</i>												
OI	87.7	98.2	95.7	92.8	94.8	99.4	95.6	99.9	95.9	95.5	92.8	99.9
opx	9.8	1.5	1.5	1.5	0.0	0.0	1.4	–	1.5	1.6	1.5	–
cpx	2.5	–	2.8	5.7	5.2	0.6	2.6	–	2.6	2.9	2.7	–
spl	–	0.3	–	–	–	–	0.4	0.1	0.1	–	3.0	0.1
<i>wt.%</i>												
SiO <sub>2</sub>	41.6	40.7	42.5	41.6	41.2	40.3	41.8	40.2	41.30	40.9	40.1	40.5
TiO <sub>2</sub>	0.09	0.07	0.10	0.11	0.18	0.19	0.20	0.04	0.18	0.07	0.12	0.02
Al <sub>2</sub> O <sub>3</sub>	0.41	0.25	0.45	0.57	0.39	0.26	0.45	0.05	0.50	0.34	0.12	0.08
FeO*	8.97	8.22	8.25	8.01	9.02	9.52	8.50	8.76	8.34	10.0	10.8	8.32
MnO	0.14	0.15	0.13	0.14	0.16	0.14	0.14	0.13	0.13	0.20	0.15	0.13
MgO	47.5	49.2	47.1	47.0	46.8	48.1	46.7	50.2	47.4	46.2	47.7	50.5
CaO	0.74	0.75	0.89	1.63	1.45	0.78	1.39	0.09	1.37	1.59	0.49	0.02
Na <sub>2</sub> O	b.d.l.	b.d.l.	b.d.l.	b.d.l.	b.d.l.	b.d.l.	b.d.l.	b.d.l.	b.d.l.	b.d.l.	b.d.l.	b.d.l.
K <sub>2</sub> O	0.10	0.19	0.06	0.46	0.28	0.10	0.19	0.01	0.25	0.25	0.04	b.d.l.
P <sub>2</sub> O <sub>5</sub>	b.d.l.	b.d.l.	b.d.l.	0.001	0.013	0.008	0.031	b.d.l.	0.037	0.003	0.002	b.d.l.
Total	99.53	99.47	99.50	99.49	99.47	99.47	99.43	99.55	99.56	99.58	99.59	99.50
LOI	0.90	3.85	3.14	4.16	4.79	3.71	3.01	0.40	2.38	2.86	2.24	0.54
<i>μg/g (ppm)</i>												
Zn	68.4	88.9	54.4	68.80	76.3	71.8	57.9	58.2	51.9	133	84.2	53.5
Cu	8.19	3.84	9.98	5.32	19.28	8.39	25.91	3.4	20.8	8.19	10.6	3.35
Ni	2359	2631	2429	2397	2264	2364	2310	2879.3	2388	2431	2365	3286
Cr	2120	2284	2272	2311	2595	2599	2973	1534.0	1742	1371	1441	1601
V	41.0	25.0	36.4	35.5	49.5	39.6	47.1	11.8	51.7	38.8	30.3	7.36
Ba	12.9	19.8	9.00	35.10	43.4	28.7	38.4	7.5	53.2	19.8	14.8	0.700
Sc	4.20	3.80	2.40	7.1	3.20	0.60	4.90	b.d.l	3.20	10.7	0.80	2.90
Co	118.11	123	120	109	109	130	113	142.45	120	116	129	135
Ga	1.64	1.094	1.11	1.923	1.55	1.495	1.46	0.55	1.46	3.10	0.922	0.334
Lu	0.01	0.004	0.005	0.009	0.009	0.009	0.010	0.00	0.012	0.009	0.009	0.005
Hf	0.24	0.166	0.146	0.544	0.328	0.342	0.334	0.08	0.374	0.299	0.152	0.029
<i>ng/g (ppb)</i>												
Os	3.64	3.62	3.12	1.85	1.58	2.59	2.63	1.46	1.95	4.27	0.59	1.33
Ir	3.45	3.61	3.81	1.82	3.10	2.52	2.58	1.27	3.54	3.08	0.79	0.87
Ru	6.01	7.85	4.54	1.38	2.21	4.43	7.07	3.97	5.27	8.84	1.86	–
Pt	4.60	3.21	5.25	1.06	0.78	1.39	1.50	0.08	1.42	3.60	0.72	1.50
Pd	2.14	1.98	6.20	0.48	2.02	1.71	5.69	0.74	1.37	9.60	0.72	0.66
Re	0.10	0.04	0.07	0.19	0.27	0.09	0.26	0.06	0.11	0.22	0.19	0.03
Total PGE	19.8	20.3	22.9	6.6	9.7	12.6	19.5	7.5	13.6	29.4	4.7	–
Total I-PGE	13.1	15.1	11.5	5.1	6.9	9.5	12.3	6.7	10.8	16.2	3.2	–
Total P-PGE	6.7	5.2	11.5	1.5	2.8	3.1	7.2	0.8	2.8	13.2	1.4	2.2
<i>Chondrite-normalized</i>												
(Pt/Pd) <sub>N</sub>	1.17	0.88	0.46	1.21	0.21	0.44	0.14	0.06	0.56	0.20	0.54	1.23
(Os/Ir) <sub>N</sub>	0.98	0.93	0.76	0.94	0.47	0.95	0.94	1.07	0.51	1.29	0.69	1.42
(Pd/Ir) <sub>N</sub>	0.51	0.45	1.35	0.22	0.54	0.56	1.82	0.48	0.32	2.58	0.75	0.63
(Pt/Ir) <sub>N</sub>	0.60	0.40	0.62	0.26	0.11	0.25	0.26	0.03	0.18	0.53	0.41	0.78
(Ru/Ir) <sub>N</sub>	1.12	1.39	0.76	0.48	0.46	1.13	1.75	2.00	0.95	1.84	1.50	–
<sup>187</sup> Re/ <sup>188</sup> Os	0.132	0.060	0.107	0.481	0.815	0.165	0.481	0.195	0.278	0.247	1.551	0.093
<sup>187</sup> Os/ <sup>188</sup> Os	0.11203	0.11148	0.12297	0.11665	0.12183	0.11213	0.11665	0.11540	0.11509	0.11144	0.11732	0.11480
γ <sub>Os</sub>	−10.0	−10.4	−1.2	−6.2	−2.1	−9.9	−6.2	−7.2	−7.5	−10.4	−5.7	−7.7
<i>Os model ages (Myr)</i>												
T <sub>Ma</sub>	3330	2769	1075	−14258	−1066	3719	−14209	3384	5325	5571	−609	2471
T <sub>RD</sub>	2313	2388	805	1681	964	2299	1680	1852	1896	2393	1589	1935
T <sub>RD</sub> erupt	2363	2410	846	1862	1274	2361	1861	1925	2000	2485	2170	1971
<sup>187</sup> Os/ <sup>188</sup> Os <sub>initial</sub>	0.11167	0.11132	0.12268	0.11533	0.11960	0.11168	0.11534	0.11487	0.11433	0.11076	0.11308	0.11454

Modes, major and element composition taken from Wittig et al. (2008a). Model ages (Myr) are calculated after Walker et al. (1989) and Pearson et al. (1995). Chondrite is taken from McDonough and Sun (1995). <sup>187</sup>Os/<sup>188</sup>Os initial is calculated for an eruption age (580 Ma, Heaman, 2005). γ<sub>Os</sub> after Meisel et al. (1996). Ru abundances were determined by ICP-MS using collision cell technology (Thermo-Scientific Xseries2).

Furthermore, FeO abundances appear enriched in some of these xenoliths (Fig. 2d) and are decoupled from other major elements. High precision whole-rock heavy rare earth element concentrations (HREE), however, clearly require the depletion of the WG-NAC SCLM to have occurred in a relatively shallow setting (≤2 to 3 GPa) akin to present-day subduction zones and/or mid-ocean ridges (Wittig et al., 2008a).

### 3. Os isotope and platinum-group element methodology

Details of Os isotope and PGE digestion and separation procedures are given in Pearson and Woodland (2000), however, our study uses a higher digestion temperature. All PGE abundances were determined by isotope dilution techniques. Approximately 1 g of whole-rock powder or olivine crystals were combined with a mixed PGE spike (<sup>190</sup>Os, <sup>191</sup>Ir,

G-06-12A	G-06-14A	G-06-14B	G-06-18A	39670	126739	126740	126742	Aver.	SD	Min	Max
98.2	98.1	95.7	93.5	–	–	–	–	96	3	88	100
1.7	1.5	1.5	5.8	–	–	–	–	2	3	0	10
–	–	2.7	0.7	–	–	–	–	3	2	1	6
0.1	0.4	0.1	–	–	–	–	–	1	1	0	3
38.9	40.0	40.9	42.3	–	–	–	–	40.9	0.9	38.9	42.5
0.09	0.17	0.29	0.07	–	–	–	–	0.1	0.1	0.02	0.3
0.04	0.20	1.29	0.17	–	–	–	–	0.3	0.3	0.04	1.3
16.5	9.03	8.00	8.00	–	–	–	–	9.3	2.1	8.0	16.5
0.20	0.16	0.15	0.11	–	–	–	–	0.1	0.0	0.1	0.2
43.8	48.9	45.7	48.3	–	–	–	–	47.6	1.7	43.8	50.5
0.34	0.94	2.15	0.63	–	–	–	–	1.0	0.6	0.02	2.1
b.d.l.	b.d.l.	b.d.l.	b.d.l.	–	–	–	–	–	–	–	–
0.04	0.11	1.02	0.05	–	–	–	–	0.2	0.3	0.0	1.0
b.d.l.	0.030	1.017	b.d.l.	–	–	–	–	0.1	0.3	0.0	1.0
99.80	99.52	99.44	99.66	–	–	–	–	99.5	0.1	99.4	99.8
–0.36	2.96	3.63	1.24	–	–	–	–	2.5	1.5	–0.4	4.8
132	76.8	63.3	57.2	–	–	–	–	74.8	25.1	51.9	132.7
16.8	9.78	20.5	8.49	–	–	–	–	11.4	7.0	3.3	25.9
1741	2557	2373	2484	–	–	–	–	2453.8	318.4	1741.3	3286.0
71	1841	2738	743	–	–	–	–	1889.7	763.8	71.4	2972.8
24.4	39.2	67.8	24.5	–	–	–	–	35.6	15.1	7.4	67.8
9.90	47.3	114	10.8	–	–	–	–	29.1	27.6	0.7	113.7
1.20	2.70	5.80	b.d.l	–	–	–	–	3.8	2.7	0.6	10.7
166.57	121.29	98.5	124	–	–	–	–	123.4	15.7	98.5	166.6
0.67	1.23	1.88	0.862	–	–	–	–	1.3	0.7	0.3	3.1
0.01	0.01	0.008	0.004	–	–	–	–	0.0	0.0	0.0	0.0
0.15	0.32	0.291	0.157	–	–	–	–	0.2	0.1	0.0	0.5
4.61	3.32	4.51	4.04	0.11	2.38	2.45	1.64	2.6	1.3	0.1	4.6
1.38	2.88	4.29	4.14	2.11	1.92	2.33	2.12	2.6	1.1	0.8	4.3
6.37	7.17	–	6.14	2.75	2.99	4.52	1.08	4.7	2.3	1.1	8.8
1.73	2.26	3.60	3.37	2.75	2.56	1.19	2.37	2.2	1.4	0.1	5.3
3.12	1.03	2.98	4.31	0.74	0.21	1.54	0.50	2.4	2.4	0.2	9.6
0.13	0.07	0.24	0.06	0.07	0.04	0.03	0.08	0.1	0.1	0.03	0.3
17.2	16.7	–	22.0	8.46	10.06	12.03	7.71	14.5	6.8	4.7	29.4
12.4	13.4	–	14.3	4.97	7.29	9.30	4.84	9.8	4.0	3.2	16.2
4.8	3.3	6.6	7.7	3.49	2.77	2.73	2.87	4.6	3.3	0.8	13.2
0.30	1.20	0.66	0.43	2.01	6.73	0.42	2.57	1.1	1.5	0.1	6.7
3.10	1.07	0.98	0.91	0.05	1.15	0.98	0.72	1.0	0.6	0.0	3.1
1.87	0.29	0.58	0.86	0.29	0.09	0.55	0.20	0.7	0.7	0.1	2.6
0.56	0.35	0.38	0.37	0.59	0.60	0.23	0.50	0.4	0.2	0.0	0.8
2.96	1.59	–	0.95	0.83	1.00	1.25	0.33	1.2	0.6	0.3	3.0
0.136	0.102	0.252	0.252	0.323	0.083	0.062	0.224	0.30	0.35	0.06	1.55
0.12581	0.11013	0.11533	0.11455	0.11624	0.11359	0.11273	0.113733	0.11549	0.004	0.11013	0.12581
1.1	–11.5	–7.3	–7.9	–6.6	–8.7	–9.4	–8.6	–7.2	3.2	–11.5	1.1
600	3359	4482	2385	6994	2601	2588	4331	1242	5643	–14258	6994
408	2571	1862	1969	1738	2100	2218	2081	1837	557	408	2571
460	2609	1957	1997	2168	2210	2299	2378	1980	545	460	2609
0.12543	0.10985	0.11464	0.11386	0.11310	0.11278	0.11213	0.11156	0.11443	0.00396	0.10985	0.12543

$^{99}\text{Ru}$ ,  $^{194}\text{Pt}$ ,  $^{106}\text{Pd}$  and  $^{185}\text{Re}$ ) and attacked for ~12 h at ~300 °C with ~2.5 mL of 12 M HCl and ~5 mL of 16 M HNO<sub>3</sub> (inverse Aqua Regia, iAR) in a high-pressure Asher (HPA-S, Anton Paar). Following this high-pressure leaching, ~5 mL of MQ water was added to the iAR before liquid is separated from residual solids by careful pipetting. The iAR was then transferred to pre-cleaned 50 mL centrifuge tubes and a total of 7 mL of carbon tetrachloride (CCl<sub>4</sub>) was applied during the course of

multiple extractions in order to separate Os from other PGEs. After each extraction (~1 h), the CCl<sub>4</sub> was transferred to pre-cleaned 15 mL Savillex Teflon vials and a new aliquot of CCl<sub>4</sub> was administered to the diluted iAR. After completion of the extractions ~4 mL of HBr was added to CCl<sub>4</sub> in order to back-extract the Os. The CCl<sub>4</sub>-HBr mixture was left on a mechanical shaker for ~6–12 h before the CCl<sub>4</sub> was removed by pipetting and the HBr was evaporated. Os was further purified by micro-

**Table 3**  
PGE and Re–Os isotope data of olivine from North Atlantic Craton peridotites (Greenland).

	Northwest						Southwest				
	488850	488850	474557	474576	474574	483606	G-06-6C	G-06-14A	G-06-12A	G-06-7A	23673
Locality	Francois NAC	Francois NAC	P-Dyke Nags.	P-Dyke Nags.	P-Dyke Nags.	Kangerlussuaq Nags.	Pyramidefjeld NAC	Pyramidefjeld NAC	Pyramidefjeld NAC	Pyramidefjeld NAC	Nigerlikasik NAC
Mg#	93.1	93.1	–	–	92.7	91.0	–	–	–	–	–
<i>ng/g (ppb)</i>											
Os	–	0.218	0.776	1.87	2.47	3.44	0.0336	1.95	4.16	0.51	2.97
Ir	0.709	0.14	0.704	1.49	2.30	0.89	0.03	0.46	1.19	0.47	3.55
Ru	0.58	1.17	1.16	1.42	1.22	9.93	0.08	0.75	5.61	0.47	5.22
Pt	0.03	0.16	0.27	0.01	0.66	1.71	0.001	0.33	1.08	0.39	3.02
Pd	0.42	2.12	0.21	0.31	0.009	0.79	2.15	1.62	0.84	0.36	0.85
Re	0.008	0.008	0.039	0.038	0.022	0.027	0.017	0.015	0.033	0.027	0.016
Total PGE	–	3.8	3.1	5.1	6.7	16.8	2.3	5.1	12.9	2.2	15.6
Total I-PGE	–	1.5	2.6	4.8	6.0	14.3	0.1	3.2	11.0	1.4	11.7
Total P-PGE	0.4	2.3	0.5	0.3	0.7	2.5	2.2	1.9	1.9	0.7	3.9
<i>Chondrite-normalized</i>											
(Pt/Pd)N	0.03	0.04	0.72	0.02	38.61	1.18	0.0002	0.11	0.70	0.59	1.93
(Os/Ir)N	–	1.41	1.02	1.17	1.00	3.58	1.18	3.95	3.25	1.01	0.78
(Pd/Ir)N	0.49	12.23	0.24	0.17	0.003	0.74	67.14	2.91	0.58	0.63	0.20
(Pt/Ir)N	0.02	0.49	0.17	0.00	0.13	0.86	0.01	0.32	0.41	0.37	0.38
(Ru/Ir)N	0.53	5.24	1.05	0.61	0.34	7.13	1.94	1.05	3.02	0.65	0.94
$^{187}\text{Re}/^{188}\text{Os}$	–	0.179	0.242	0.098	0.042	0.038	0.029	0.036	0.039	0.273	0.026
$^{187}\text{Os}/^{188}\text{Os}$	–	0.10732	0.11022	0.10719	0.10871	0.10995	0.11027	0.10814	0.12585	0.11014	0.11044
$\gamma$ Os	–	–13.74	–11.41	–13.84	–12.62	–11.63	–11.37	–13.08	1.15	–11.47	–11.24
<i>Os model ages (Myr)</i>											
T Ma	–	4788	5793	3834	3060	2844	2738	3099	442	6950	2688
T RD	–	2813	2559	2968	2763	2596	2552	2841	402	2569	2530
T RD erupt	–	3048	2877	3096	2818	2646	2562	2854	416	2670	2542
$^{187}\text{Os}/^{188}\text{Os}$ initia	–	0.10660	0.10787	0.10624	0.10830	0.10958	0.11019	0.10804	0.12579	0.10940	0.11034

Model ages (Myr) are calculated after Walker et al., 1989 and Pearson et al. (1995). Chondrite is taken from McDonough and Sun (1995).  $^{187}\text{Os}/^{188}\text{Os}$  initial is calculated as eruption age (580 and 164 Ma for northern and southern localities, Heaman, 2005). All olivine separates were digested using a high-Pressure Asher.  $\gamma$ Os after Meisel et al. (1996). NAC and Nags. denote North Atlantic Craton and Nagsuqtoqidian mobile belt (Fig. 1) Ru abundances were determined by ICP-MS using collision cell technology (Thermo-Scientific Xseries2). Mg# ( $\text{Mg}/[\text{Mg} + \text{Fe}] \times 100$ ) after Sand et al. (2009).

distillation (~2 h, 90 °C) utilizing 20  $\mu\text{L}$   $\text{H}_2\text{CrO}_4$  and 20  $\mu\text{L}$  6 M  $\text{H}_2\text{SO}_4$ . The samples were then removed from the hotplate and the  $\text{H}_2\text{CrO}_4$ – $\text{H}_2\text{SO}_4$  mixture was discarded while an additional 10  $\mu\text{L}$  of HBr was added to collect Os from the conical beaker walls. Subsequently, the HBr was evaporated to near dryness (~0.5  $\mu\text{L}$ ) and then loaded onto Pt filaments and a  $\text{Ba}(\text{OH})_2$  activator was applied before the samples were run for Os isotopes on a Thermo-Scientific Triton thermal ionisation mass spectrometer at Durham.

Total procedural blanks yield an average  $^{187}\text{Os}/^{188}\text{Os}$  of 0.15 and total Os blanks of <4 pg using quartz HPA reaction vials dedicated to peridotites. The in-house mass spectrometry standard UMCP-3 (load size tailored to yield similar signal sizes to samples; 0.17 ng,  $n = 19$ ) run over an 18 month period yielded  $^{187}\text{Os}/^{188}\text{Os}$  of  $0.1138 \pm 2$  and a reproducibility of 1.6%, which is in excellent agreement with the long-term in-house multi-user Os isotope reproducibility of 2.2 % yielding an average  $^{187}\text{Os}/^{188}\text{Os}$  of  $\sim 0.1138 \pm 3$ . A smaller number of the international Os isotope mass spectrometry standard DROsS (load size 0.1 ng,  $n = 7$ ) yielded  $^{187}\text{Os}/^{188}\text{Os} \sim 0.1608 \pm 5$ , which agrees well with previously published data (Luguet et al., 2008). Replicate digestions of the in-house peridotite standard GP13 yields 1.7% reproducibility for Os isotopes and ~5% RSD for Os abundances ( $n = 10$ ,  $^{187}\text{Os}/^{188}\text{Os} \sim 0.12605 \pm 19$ ,  $\text{Os} \sim 3.78$  ppb: Table A, supplementary data file), which is in excellent agreement with previously published data (e.g., Pearson et al., 2004).

After the removal of Os, PGEs were further purified by transferring the iAR to pre-cleaned 22 mL Savillex Teflon vials and evaporating the liquid. The samples were taken up in 10 mL of 0.5 M HCl and centrifuged in order to avoid loading solids onto the anion-exchange columns used to remove the sample matrix and to separate the PGEs into cuts containing Pd and Ir, Pt, Ru, and also Re, respectively. Half of the sample solutions were loaded (5 mL of 0.5 M HCl) and 10 mL of 1 M HF/1 M HCl

and 0.8 M  $\text{HNO}_3$  were eluted to remove most of the sample matrix. Ir, Pt, Ru and Re were then collected in 10 mL of 13.5 M  $\text{HNO}_3$  before a further 40 mL of 1 N HF/1 N HCl was administered in order to completely remove the sample matrix. Pd was then collected in 20 mL of 9 N HCl. Both, the Ir–Pt–Ru–Re and the Pd cut were dried down, and taken up in 1 mL of 0.5 N HCl and transferred into centrifuge tubes.

Os concentrations were calculated from TIMS mass spectrometry, whereas Ir, Pt, Pd and Re concentrations were determined using an Element 2 ICP-MS. Details of these mass spectrometry procedures are given in Dale et al. (2008). All PGE concentrations were corrected for total procedural blank contributions. The reproducibility of Ir, Pt and Pd abundances in GP13 is ~10% RSD, whereas Re has an uncertainty of 3% RSD (Table A, supplementary data file). As a result of the high susceptibility of the Element 2 to the formation of polyatomic Cr-based interferences on  $^{101}\text{Ru}$  during Ru ID measurements, which cripple the accurate and precise acquisition of Ru abundance data in some peridotite runs, all Ru abundances presented here were determined using second generation collision cell technology of the Thermo-Scientific Xseries2 ICP-MS. Ru concentrations from this mass spectrometry methodology are precise within 5% RSD, while Ru data for GP13 attest to an accuracy of ca. 10% RSD (Table A, supplementary data file).

#### 4. Results

The PGE abundances and Re–Os isotope systematics of the WG-NAC peridotites and constituent olivines are given in Tables 1, 2 and 3. Description of the PGE systematics of the different northern regions will be dealt with together as a result of their similar PGE abundances and Os systematics (Section 4.1, see also Webb, 2007); whereas the southern locality will be described separately because

of the distinctly different PGE systematics relative to the northern samples (Section 4.2).

#### 4.1. Re–Os isotope ratios and platinum-group element abundances of northern WG–NAC and Nagssuqtoqidian peridotites

The samples from the northern WG–NAC and the Nagssuqtoqidian mobile belt have highly variable Os, Ir and Ru abundances (I–PGE) ranging from 0.05 to 6.1 ng/g, 0.7 to 5.4 ng/g and 0.3 to 10.9 ng/g, respectively. Mean values of Os, Ir and Ru are  $2.7 \pm 1.5$  ng/g,  $2.6 \pm 1.3$  ng/g and  $5.0 \pm 2.8$  ng/g, respectively (Fig. 3). There is no statistically relevant mode in Os and Ir abundances (supplementary data file, Figs. A, B). These mean Os and Ir abundances are somewhat lower than estimates of Prima (primitive mantle, McDonough and Sun, 1995, see also Table A) or residual mantle based on other cratonic xenoliths suites from Lesotho, Somerset Island and the Slave Province (Fig. 3, Irvine et al., 2003; Pearson et al., 2004) that have experienced large degrees of melt extraction. The samples typically show little I–PGE fractionation although the entire range of  $[\text{Os}/\text{Ir}]_N$  is 0.4 to 2.9, which is larger than typical for cratonic peridotites. This range is more consistent with off-craton SCLM (Handler and Bennett, 1999; Lorand and Alard, 2001; Lorand et al., 2003; Pearson et al., 2004; Wittig et al., 2010a and references therein). P–PGE abundances (Pd, Pt) are also highly varied and range from 0.03 to 10.0 ppb and 0.01 to 5.4 ppb for Pt and Pd, respectively although most samples have low P–PGE concentrations (supplementary data file, Figs. A, B, <1 ng/g, ca. 75%) that are distinctly lower than Prima. Median WG–NAC P–PGE abundances are lower compared to other cratonic peridotites (Fig. 3). The I–PGE/P–PGE fractionation translates into generally low  $[\text{Pd}/\text{Ir}]_N$  although the entire range is 0.002 to 2.4 (Fig. 4).

Re abundances in northern WG–NAC peridotites range between 0.01 and 1.6 ng/g and appear high when compared with corresponding P–PGEs (Fig. 5). Overall, the northern WG–NAC peridotites can be grouped according to their chondrite-normalized PGE patterns into (a) those with no Os–Ir fractionation and high  $[\text{Pt}/\text{Pd}]_N$  (Fig. 5b), (b) those with no Os–Ir fractionation and low or close to unity  $[\text{Pt}/\text{Pd}]_N$  (Fig. 5c) and (c) those with more fractionated I- and P–PGE ratios (Fig. 5d). Notably, the northern WG–NAC peridotites showing P–PGE depletion ( $n=45$ , Fig. 5b and c) are marked by variable Ru abundances that result in no (ca. 25%), positive (ca. 50%) and also negative (ca. 25%) Ru anomalies relative to Ir on normalized plots. The variable Ru abundances are not correlated with other PGE abundances, major elements or trace elements. Overall, the P–PGE depleted peridotites have PGE systematics, including highly variable Ru, reminiscent of I–PGE alloys (Cabri, 2002; Shi et al., 2007). Notably, PGE abundances do not correlate with major elements such as Al (see supplementary data file, Fig. C) and Mg. An exception is FeO, which does correlate positively with Pd,  $[\text{Pd}/\text{Ir}]_N$  and also with Os model ages (Fig. 4, Fig. C [supplementary data file]). Inter-element PGE fractionation does not correlate with Yb, Lu or Hf (Fig. C in supplementary data file).

Os isotope systematics of the northern peridotites are highly varied and range from 0.10676 to 0.12811 (Fig. 6) although the majority of peridotites have  $^{187}\text{Os}/^{188}\text{Os}$  less radiogenic than 0.117. The range of  $^{187}\text{Re}/^{188}\text{Os}$  for a suite of peridotites is remarkable (0.015–6.8) but there is no clear isochronous relationship (Fig. 6, supplementary data file Fig. D). The only discernible correlation between PGE systematics and Os isotopes within the northern peridotites is that high  $[\text{Pd}/\text{Ir}]_N$  are coupled with radiogenic Os isotopes (Fig. 4).

In terms of model ages, overall, these peridotites have a high frequency of 2.7 to 3.2 Gyr  $T_{\text{RD}}^{\text{RuPt}}$  model ages and a smaller number of model ages of ca. 2.0 Gyr (Fig. 2).  $T_{\text{MA}}$  model ages (Fig. 7), yield markedly older, and sometimes unrealistic, ages relative to the more conservative  $T_{\text{RD}}^{\text{RuPt}}$  model ages (Figs. 2, 4, 7; see our supplementary data file, Section 5.3.1, Pearson et al., 2003 and Rudnick and Walker, 2009 for detailed explanations of the different Os isotope model age concepts).

#### 4.2. Re–Os isotope ratios and platinum-group element abundances of southern WG–NAC peridotites

Os, Ir and Ru abundances in mantle xenoliths from the southern Pyramidefjeld locality range from 0.1 to 4.6 ppb, 0.1 to 4.3 ppb and 1.1 to 8.8 ppb, respectively. These I–PGE abundances are on average similar to the northern WG–NAC samples, but lower than in other cratonic peridotites or values anticipated for Prima (Fig. 3). The degree of I–PGE fractionation is similar to the northern peridotites. Mean values of Os, Ir and Ru are  $2.6 \pm 1.3$  ppb,  $2.6 \pm 1.1$  ppb and  $4.7 \pm 2.3$  ppb, respectively. Overall, these peridotites lack the very low P–PGE abundances that are typical in the northern peridotites and instead exhibit Pd enrichment (Pt 0.1–5.3 ppb, Pd 0.2–9.6 ppb, Figs. 4, 8 and supplementary data file Fig. A, B). Re abundances in southern peridotites range between 0.03 and 0.27 ppb and often appear elevated when compared to corresponding P–PGEs. Chondrite-normalized PGE patterns are diverse in these peridotites (Fig. 8), while  $[\text{Pd}/\text{Ir}]_N$  ranges from 0.2 to 0.6 (Fig. 4). PGE abundances do not correlate with major elements such as Al (see supplementary data file, Fig. C) and Mg. The exception is FeO, which correlates positively with Pd,  $[\text{Pd}/\text{Ir}]_N$  and also with Os isotopes and hence Os model ages (Fig. 4, Fig. C [supplementary data file]). PGE inter-element fractionation ( $[\text{Pd}/\text{Ir}]_N$ ) do not correlate with other potential melt depletion indicators such as Yb, Lu and Hf abundances (Fig. C in supplementary data file).

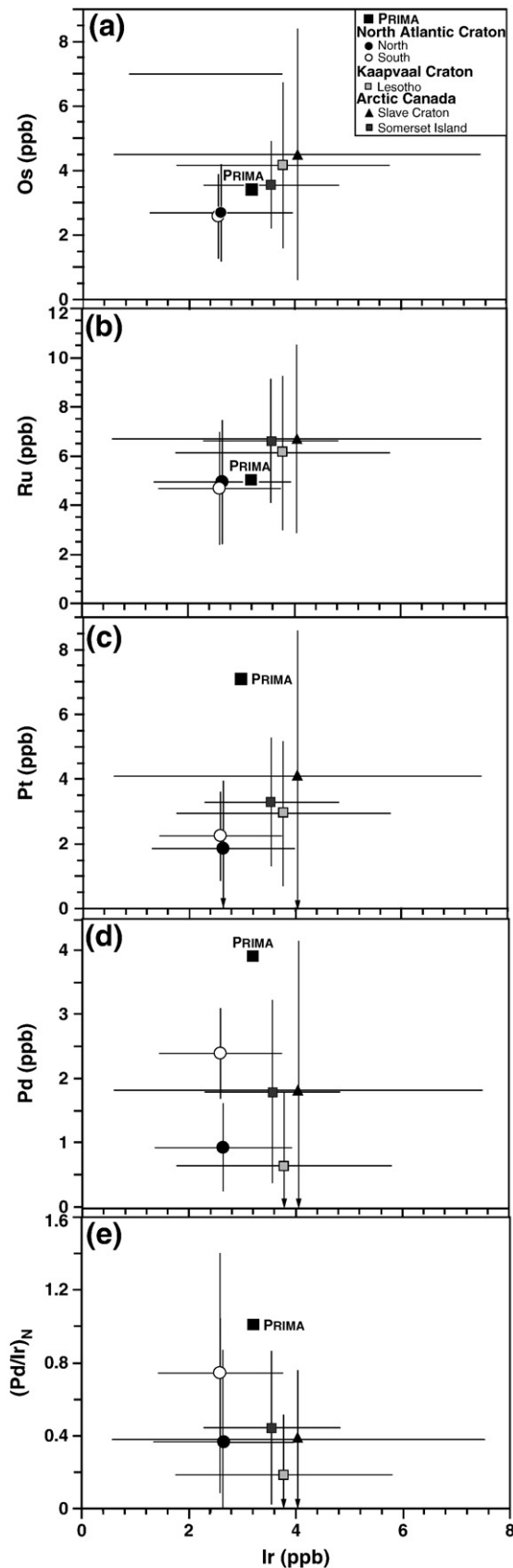
The southern peridotites have more radiogenic Os isotopes than their northern counterparts, ranging from  $^{187}\text{Os}/^{188}\text{Os}$  0.11013 to 0.12581 (Fig. 6) and there is no correlation with  $^{187}\text{Re}/^{188}\text{Os}$  (0.06–1.6, Fig. 6 and supplementary data file Fig. D). Overall, the southern peridotites yield  $T_{\text{RD}}^{\text{RuPt}}$  model ages that cluster at ca. 2 and between 2.3 and 2.6 Gyr (Figs. 2, 4, 7, and 9) and are coupled with relatively high  $[\text{Pd}/\text{Ir}]_N$  (Fig. 4).

#### 4.3. PGE abundances and Os isotope systematics in selected olivine separates from peridotites of the northern and southern WG–NAC

Chondrite-normalized PGE patterns for olivine-whole-rock pairs of peridotites from the northern WG–NAC vary widely between samples (Fig. 10), although some features can be generalized. Overall, constituent olivine separates have I–PGE and Pt abundances that are lower than the corresponding whole-rock peridotites. In most instances, chondrite-normalized PGE patterns for olivines match those of their host rocks. An exception is olivine from sample 474576, which has higher I–PGE and Pd abundances than the corresponding whole-rock. Os and Ir in these olivines is sometimes fractionated ( $[\text{Os}/\text{Ir}]_N \geq 1$ , Fig. 10), as observed in whole rocks. The olivines from northern peridotites show two types of P–PGE systematics; those with  $[\text{Pd}/\text{Pd}]_N < 1$  (474574, 483606) and those that show Pd enrichment relative to Pt (474576, 474557, 488850). Os isotope ratios in these northern peridotite olivines range between  $^{187}\text{Os}/^{188}\text{Os}$  0.10719 and 0.11022, i.e., at the unradiogenic end of the whole-rock range. Overall,  $T_{\text{RD}}^{\text{RuPt}}$  model ages of whole rocks and constituent olivines agree reasonably well with each other, except for 474557 (Fig. 10).

Chondrite-normalized PGE patterns for olivine-whole-rock pairs of peridotites from Pyramidefjeld (southern WG–NAC) show that the olivines from this locality have lower I–PGE abundances than their northern counterparts. In addition, Pt abundances are relatively low while Pd concentrations appear somewhat elevated. Except for olivine from the highly metasomatised, dunitic sample G–06–12a, these olivines yield relatively unradiogenic  $^{187}\text{Os}/^{188}\text{Os}$  between 0.10814 and 0.12585 resulting in  $T_{\text{RD}}^{\text{RuPt}}$  model ages older than the corresponding whole rocks.

A single olivine separate from a dunite xenolith from the Nigerlikasik locality, closer to the central part of the exposed craton, exhibits I–PGE abundances similar to these found in the northern WG–NAC whole rocks (Fig. 10). I–PGE abundances are substantially higher than P–PGEs and Re. This sample has a  $^{187}\text{Os}/^{188}\text{Os}$  of 0.11044 yielding a 2.54 Gyr  $T_{\text{RD}}^{\text{RuPt}}$  model age.



## 5. Discussion

### 5.1. Disparate PGE and Os isotope systematics in northern and southern North Atlantic Craton peridotites

A first order observation is that the degree of serpentinization experienced by these xenoliths is substantially more extreme in the northern peridotites relative to those from the southern locality of Pyramidefjeld (Wittig et al., 2008a). A second distinction is the eruption age of the host volcanic rocks. The kimberlites and UMLs that sampled the northern WG-NAC SCLM erupted in the Neo-Proterozoic, while those providing mantle xenoliths around Pyramidefjeld intruded into the southern TTG-granite crust during the Mesozoic (Heaman, 2005; Tappe et al., 2007) thus leaving a longer window for metasomatic alteration in the South. Despite the disparity in degree of serpentinization and eruption age of the host volcanic rocks, major and trace elements in the northern and southern peridotites are equally variable and overall show high levels of depletion (Wittig et al., 2008a). However, PGE and Os isotope systematics reveal significant differences between the samples from the northern and southern margin of the WG-NAC (Figs. 5–10).

The majority of northern peridotites are marked by very low P-PGE abundances ( $n=30$ ;  $\sim 83\%$ , Figs. 5 and 10). These P-PGE depleted samples can be found in all northern localities (“Kangerlussuaq”, “Sarfartoq”, “Maniitsoq”, Figs. 1 and 9). The low P-PGE abundances are accompanied by unradiogenic Os isotopes and  $T_{RD}^{erupt}$  model ages  $\geq 2$  Gyr. The remainder of the northern peridotites ( $n=6$ ) also originate from all three northern kimberlite clusters and have elevated Pt and Pd abundances relative to most of these samples. All of these Pd-enriched samples have post-Archean  $T_{RD}^{erupt}$  model ages with some exhibiting model ages of ca. 2 Gyr ( $n=2$ ) or between 1.2 and 1.4 Gyr ( $n=2$ ). The P-PGE depletion of the majority of northern WG-NAC peridotites is similar to that seen in peridotites from cratonic continental mantle roots of the Kaapvaal and Slave Craton as well as Somerset Island (Irvine et al., 2003; Pearson et al., 2004). Given the correlation of low P-PGE abundances with unradiogenic Os isotopes seen in northern WG-NAC samples it seems that PGE systematics and derived Os model ages are systematically related and most likely stem from large-scale melt extraction early in the evolution of the WG-NAC (Fig. 4 and Fig. C in supplementary data file). This has been suggested in order to explain the low P-PGE abundances of other Archean continental mantle (Pearson et al., 2004). However, in detail, the northern WG-NAC peridotites appear to have lower I-PGE concentrations compared with previously studied Archean SCLM (e.g., Irvine et al., 2001; 2003; Pearson et al., 2004). The melting behaviour of PGEs will be further examined in Section 5.2.

Peridotites from the southern WG-NAC generally have higher Pd abundances than those from the northern WG-NAC and other cratonic continental mantle roots (Figs. 3, 4, 5 and 8). Chondrite-normalized PGE patterns appear variable with only few samples exhibiting P-PGE troughs that are characteristic of the northern peridotites (Figs. 5 and 8). Unsurprisingly, Archean  $T_{RD}^{erupt}$  model age is extremely rare in these southern peridotites. The remaining samples have post-Archean  $T_{RD}^{erupt}$  model ages and no specific PGE pattern can be associated with their Os isotope composition. Overall, the high Pd abundances appear to record Pd introduction due to metasomatism.

**Fig. 3.** Median Os (a), Ru (b), Pt (c), Pd (d) concentrations (ng/g) and [Pd/Ir]<sub>N</sub> (e) versus Ir (ng/g) comparing northern and southern WG-NAC with primitive mantle (Prima), and averages of whole-rock peridotites from Somerset Island and the Slave and Kaapvaal craton. Data taken from Pearson et al. (2004), Irvine et al. (2001; 2003). Prima after McDonough and Sun (1995). Note the similarities of the northern and southern WG-NAC median concentrations in Os-, Ru-, Pt-Ir space that are generally lower than other Archean continental mantle roots, however, Pd and [Pd/Ir]<sub>N</sub> systematics differ in these northern and southern WG-NAC peridotites markedly. For convenience, we present the PGE abundances of the northern (and southern) WG-NAC peridotites as histograms in the supplementary data of this contribution.

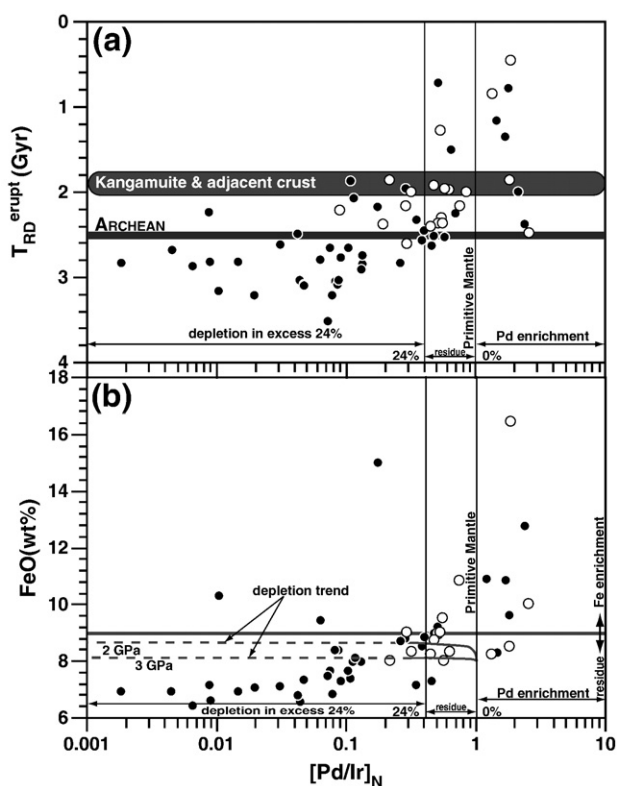


**Fig. 4.**  $T_{RD}^{erupt}$  Os model ages (a) and FeO (b) versus  $[Pd/Ir]_N$  of northern and southern WG-NAC whole-rock peridotites. Also shown is the  $[Pd/Ir]_N$  of primitive mantle (Prima) and a 24% depleted residue calculated from Prima using model parameters of Pearson et al. (2004). Note that the majority of northern WG-NAC samples have  $[Pd/Ir]_N < 1$ , Archean  $T_{RD}^{erupt}$  model ages (a) and FeO abundances consistent with melt extraction ( $FeO < 9$  wt.%, b, depletion parameter after Herzberg, 2004). A sub-fraction of these peridotites has model ages of ca. 2 Gyr; the age of Kangamuit dyke intrusion and formation of continental crust adjacent to the WG-NAC, depleted  $[Pd/Ir]_N$  (a) and FeO between 8 and 9 wt.% (b). A minority of northern samples, however, have experienced Pd and Fe enrichment associated with more radiogenic Os isotopes and “young”  $T_{RD}^{erupt}$  model ages. Southern WG-NAC peridotites have higher Pd and FeO abundances compared to the bulk of the northern samples. They typically possess somewhat more radiogenic Os isotopes resulting in  $T_{RD}^{erupt}$  model ages younger than 2.5 Gyr.

In summary, northern WG-NAC peridotites are marked by melt extraction-related P-PGE depletion that is generally absent in the samples from the south (Figs. 5, 8, 9 and 10). Unradiogenic Os isotopes are accompanied by P-PGE depleted PGE patterns and  $T_{RD}^{erupt}$  model ages are generally Archean in the north, whereas the southern margin whole-rock peridotites have more radiogenic Os isotopes and give  $T_{RD}^{erupt}$  model ages that are typically Paleoproterozoic in age.

## 5.2. The northern WG-NAC: a siderophile perspective on Archean mantle depletion

The matter of melt depletion in peridotites has been a focus of mantle petrologists and geochemists for decades. A wide variety of major and trace elements have been proposed as proxies for the degree of melt extraction and also for melting depths (for an overview see Pearson et al., 2003). At the same time, it has been recognized that lithophile elements in peridotites and their constituent silicates are ubiquitously affected by metasomatic alteration (e.g. Menzies and Hawkesworth, 1987). The lithophile elements of the WG-NAC peridotites were examined in detail by Wittig et al. (2008a). The very low concentrations of elements that are relatively robust to metasomatism such as Yb, Lu (<0.03 ppm) and Hf indicate that depletion occurred dominantly at low

pressure, in a mid-ocean ridge or subduction zone setting (2 to 3 GPa) because melting at greater depth (e.g. 7 GPa,) would occur in the presence of high modal amounts of garnet (ca. 20%; Walter, 2003), retaining more HREE in the residual peridotites ( $Lu > 0.06$  ppm). Such high Lu and Yb concentrations are absent from cratonic SCLM even when Yb, Lu and Hf abundances record up to 10% of metasomatic enrichment (Wittig et al. 2008a). Despite the relative coherency within some lithophile element groups, there is no correlation between these elements and any PGE systematics (supplementary data, Fig. C). This lack of geochemical coupling may be because the metasomatic enrichment that has affected the lithophile elements is different in nature to the metasomatic processes that control highly siderophile elements (see below). Therefore, in this section we will focus on the melting behaviour of sulphides and PGE entirely to estimate the likely degree of depletion recorded by the WG-NAC SCLM.

The behaviour of sulphides and consequently that of PGEs during mantle melting has received much attention in recent years (e.g., Handler and Bennett, 1999; Luguet et al., 2003; Bockrath et al., 2004; Pearson et al., 2004; Lorand et al., 2008), often in conjunction with studies of Os isotopes. While early whole-rock Os isotope studies of mantle peridotites produced clear evidence of the Archean heritage of cratonic lithosphere, later studies noted the likely disturbance of some samples (Carlson and Irving, 1994; Carlson and Moore, 2004; Chesley et al., 2004; Pearson et al., 1995; 2004; Walker et al., 1989). Studies of sulphides (e.g., Alard et al., 2002; Griffin et al., 2004; Lorand and Gregoire, 2006) clearly showed the presence of some metasomatic sulphides in many peridotites, while in very depleted peridotites alloy phases are likely to be more important hosts for I-PGE and Pt (Luguet et al., 2007) with sulphides being rare. Pearson et al. (2004) have shown that a combination of whole-rock PGEs and Os isotopes in cratonic peridotites can be used to constrain original melting signatures and a review of recent studies by Rudnick and Walker (2009) confirms the usefulness of this approach. Consequently, PGE and Os isotope systematics have been combined to determine which WG-NAC peridotites may have retained their original melting age.

PGEs are hosted in the sulphide fraction of fertile and mildly depleted peridotites. These sulphides constitute only a minute percentage of the modal abundances of peridotites (<1%, e.g. Hart and Gaetani, 2006) if 250 ppm sulphur in primitive mantle is assumed (McDonough and Sun, 1995; Bockrath et al., 2004). Consequently, the behaviour of PGEs during melt extraction is determined by the evolution of less than 1% of the mineralogy of primitive mantle. Petrographic observations appear to indicate that mantle sulphides may melt incongruently, thereby removing P-PGEs more readily than I-PGEs, which remain in the evolving residue with more residual sulphides (e.g. Luguet et al., 2001, 2003 and reference therein). Experimental data on the other hand indicate that two sulphide phases may coexist in the upper mantle, which preferentially host I- and P-PGEs, respectively (Bockrath et al., 2004), with the latter being more incompatible during the melt extraction process. Although (two-)sulphide melting models may be construed as simple systems to monitor during the process of mantle melting, the heterogeneous distribution of these phases (nugget effect) means that even pristine mantle residues may exhibit significant PGE abundance variability. In addition, the evolution of this small portion of sulphides and the physical conditions of the upper mantle are difficult to reconstruct during experimental studies. Despite these difficulties, the petrographic and experimental observations both indicate that P-PGE depletion in peridotites results from the depletion process. Major and trace elements in Archean SCLM peridotites record extreme depletion of up to 40%, i.e. well beyond the sulphide stability after mantle melting to such degrees. Such samples also show extreme P-PGE depletion that can be modelled, at least to some extent, using

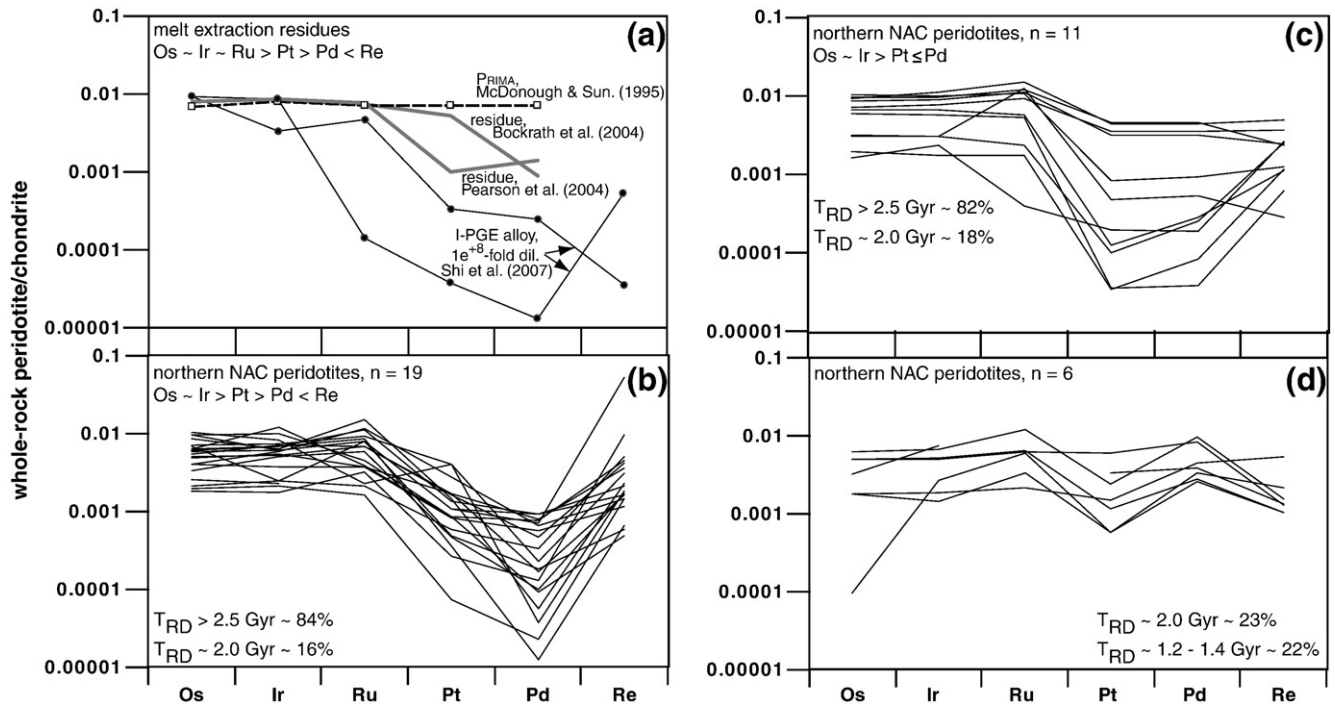


**Fig. 5.** In (a) the chondrite-normalized PGE patterns and Re of Prima (McDonough and Sun, 1995), two estimates of depleted peridotite based on Prima (Bockrath et al., 2004; Pearson et al., 2004) and I-PGE-rich alloys ( $1e^{+8}$  dilution factor, Shi et al., 2007) with positive and negative Ru anomalies are shown. These data are compared to the northern WG-NAC whole-rock peridotites from the northern margin of the WG-NAC (b–d) plotted according to the degree of fractionation of I-PGEs but also “internal” I- and P-PGE fractionation. Also given in (b) to (d) is the distribution (in per cent) of  $T_{RD}^{erupt}$  Os model ages that are older than 2.5 Gyr, those with ages of ca. 2.0 Gyr and those close to the 1.2 and 1.4 Gyr range. Chondrite after McDonough and Sun (1995). b) Northern WG-NAC peridotites, PGE patterns indicate very high degrees of melt extraction. These samples have no or only little Os–Ir fractionation, I-PGE concentrations are substantially higher than those of P-PGEs and Pd is the most depleted PGE. Overall these PGE patterns are very similar to those from I-PGE alloys, including the seemingly elevated Re. (c) Northern WG-NAC peridotites, these samples are basically similar to those in (b) except Pd abundances are equal or slightly higher than Pt. (d) Northern WG-NAC peridotites with PGE fractionation that result in PGE patterns inconsistent with mantle melting.

partial melting theory. Bockrath et al. (2004) and Pearson et al. (2004) presented melting models that generate highly depleted P-PGE abundances relative to those of I-PGEs.

Because of the very high sulphide/melt  $K_D$  for siderophile elements, PGE abundances are anticipated to remain unchanged during the initial stages of melt extraction where sulphide is still stable up until ~15% melt depletion, depending on the mantle sulphur content, sulphur solubility model and efficiency of removing high-density sulphide melts. Additional melting leads to the consumption of primary base metal sulphides and crystallization of residual sulphide (e.g., laurite [Os, Ir, Ru]S<sub>2</sub>), which

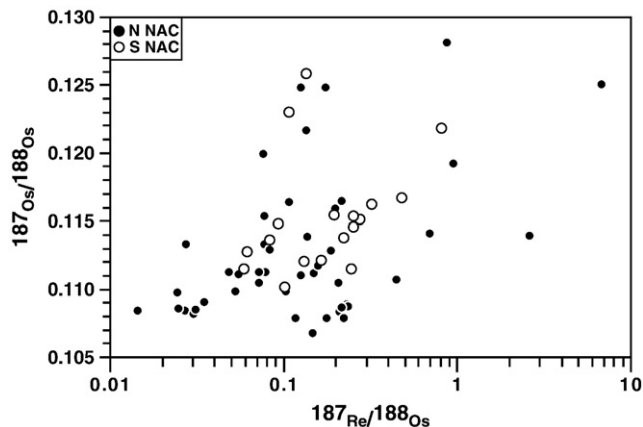


**Fig. 6.**  $^{187}Os/^{188}Os$  versus  $^{187}Re/^{188}Os$  of whole-rock WG-NAC peridotites. Note the logarithmic x-axis ( $^{187}Re/^{188}Os$ ) and the lack of isochronous correlation. In the supplementary data file we show  $^{187}Os/^{188}Os$  versus  $^{187}Re/^{188}Os$  of the individual northern WG-NAC localities.

sequester I-PGEs. This and the volume loss during melting result in elevated I-PGE abundances relative to PRIMA in residual mantle (Figs. 5 and 8). Bockrath et al. (2004) proposed that Pt and Pd are physically removed from the residue in immiscible sulphide droplets together with large volumes of Mg-rich melt, thus leaving a P-PGE depleted mantle. This PGE evolution during mantle melting is illustrated in Figs. 4, 5, and 11. Also modelled on these

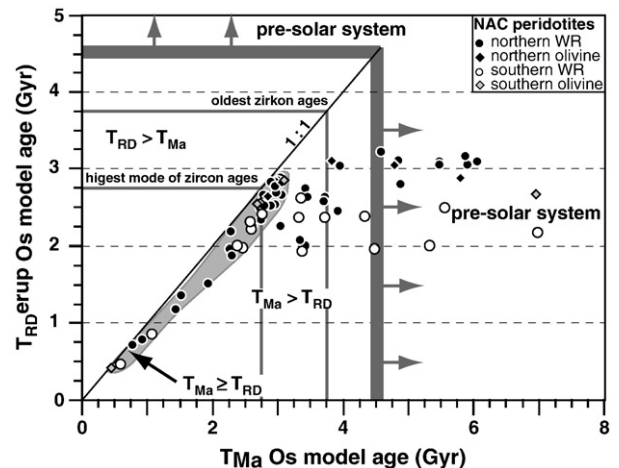


**Fig. 7.** Comparison of  $T_{RD}^{erupt}$  and  $T_{Ma}$  model ages of northern and southern WG-NAC peridotites and associated olivines. Model ages are calculated after Walker et al. (1989) and Pearson et al. (1995). Typically, both types of model ages agree with each other within a 0.2 Gyr window, although a number of samples with  $T_{RD}^{erupt}$  older than ~1.8 Gyr have substantially older  $T_{Ma}$ . Importantly, all samples with  $T_{RD}^{erupt}$  older than ~2.8 Gyr have older  $T_{Ma}$  model ages that exceed the age of the oldest solar system solids (Baker et al., 2005).

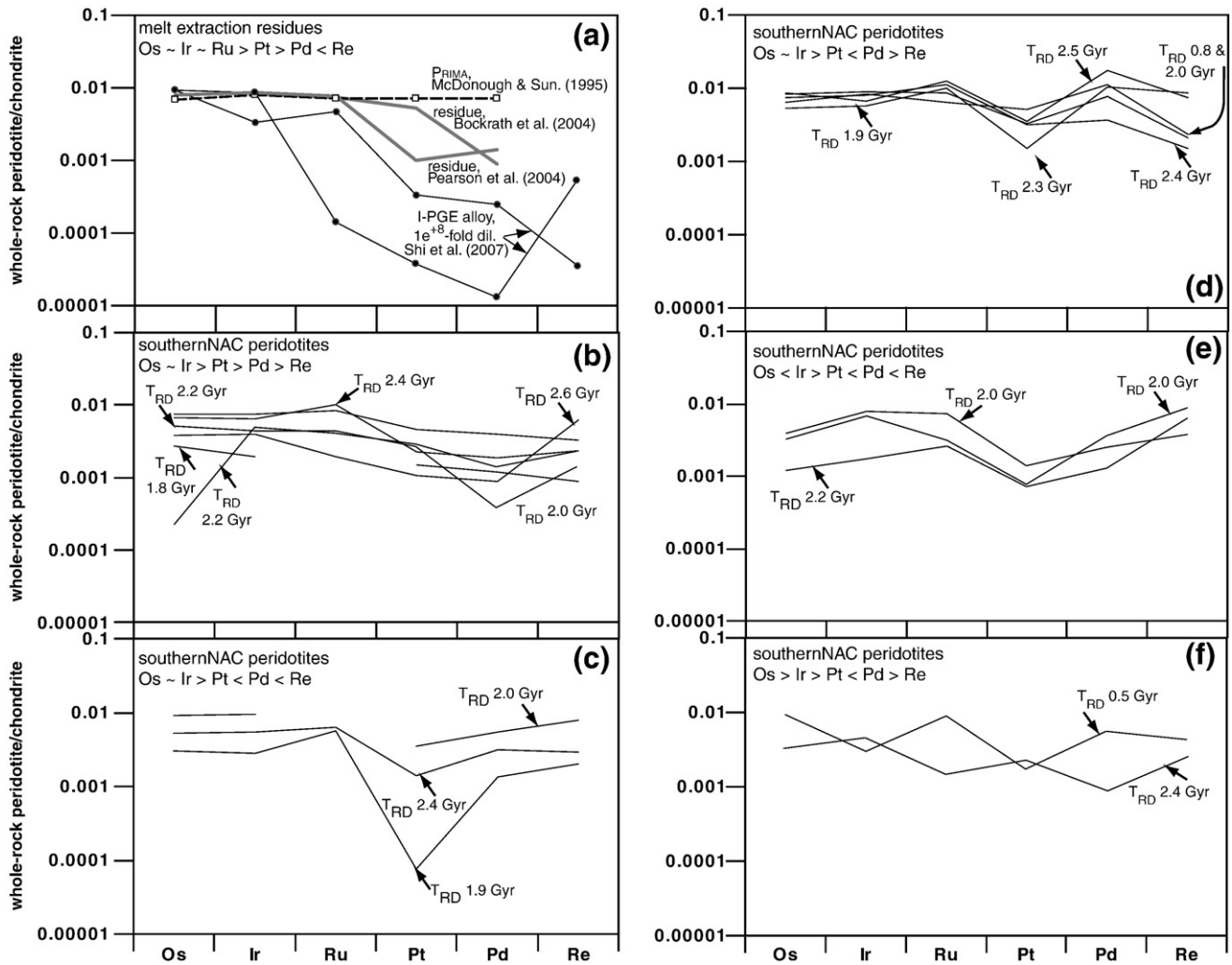


**Fig. 8.** Chondrite-normalized PGE patterns of whole-rock peridotites from the southern margin of the North Atlantic Craton plotted according to the degree of fractionation of I-PGEs from P-PGEs (b–f). The  $T_{RD}^{enriched}$  Os model ages of the individual samples are given as well. Chondrite after McDonough and Sun (1995). (a) PGE patterns and Re for mantle melting residues, based on Prima (McDonough and Sun, 1995), modelled after Pearson et al. (2004) and Bockrath et al. (2004). Also shown are two scaled down I-PGE alloy patterns taken from Shi et al. (2007), the dilution factor to approximately match the most depleted samples from the north is  $1^{e+8}$ . (b) Southern WG-NAC peridotites, these samples have PGE patterns that are either similar to those from the north ( $Os \sim Ir > Pt \geq Pd < Re$ ), or are flat with consistently decreasing normalized abundances from Os to Re. (c) Southern WG-NAC peridotites exhibiting Pt depletion and  $Os \sim Ir > Pt < Pd < Re$ . (d) Southern WG-NAC peridotites exhibiting marked Pd enrichment and  $Os \sim Ir > Pt < Pd > Re$ . (e) Southern WG-NAC peridotites with I-PGE fractionation and marked Pd and Re enrichment. (f) Southern WG-NAC peridotite with  $Os > Ir > Pt < Pd > Re$ .

diagrams is the evolution of a residue using more conventional melt depletion models (e.g., Pearson et al., 2004). The melting model relies on a primitive mantle sulphur content of 250 ppm resulting in the disappearance of sulphides during melting extraction at 24%, although lower sulphur contents have been proposed for primitive mantle, which would obviously result in an earlier exhaustion of sulphides during depletion.

Assuming a relatively shallow melting regime (2–3 GPa) as proposed for the WG-NAC peridotites by Wittig et al. (2008a) and the experimental constraints provided by Bockrath et al. (2004), which predict complete sulphide depletion at 24%, clinopyroxene is also at the verge of exhaustion. In Archean SCLM formation models, extensive melting is required to fully consume clinopyroxene and continue at the expense of orthopyroxene and olivine, possibly in a hydrous melting regime, which may allow total fractions of melt depletion up to 40% (Bernstein et al., 2006b; Pearson and Wittig, 2008; Wittig et al., 2008a). Melting in a sulphide-absent environment cannot be approximated with our PGE melting model and, at present, there is little relevant experimental data to constrain PGE behaviour at this extreme degree of depletion. However, we may anticipate that

with the removal of sulphides, PGEs may further be sequestered into alloys in refractory peridotites (Luguet et al., 2007).

In the light of these models, we can now examine the PGE systematics of the majority of northern WG-NAC peridotites (Fig. 5b and c) and a subset of southern peridotites (Fig. 7b). The budget of I- and P-PGEs in the majority of WG-NAC samples is distinctly below that expected from melting residues (Fig. 11). In addition, the northern peridotites have up to 3 orders of magnitude lower  $[Pd/Ir]_N$  ratios than the sulphide disappearance threshold derived from the sulphide melting model (Fig. 11). The marked P-PGE depletion of the WG-NAC peridotites is also found in other Archean SCLM (Figs. 3 and 11). The chondrite-normalized PGE patterns of northern peridotites with fractionated, low  $[Pd/Ir]_N$  (and other Archean SCLM with these characteristics) mirror those of the modelled melting residues and are simply displaced towards lower PGE abundances (Fig. 5). Platinum-group alloys (PGAs), enriched in I-PGE exhibit the same P-PGE depletion relative to I-PGE and Re (Shi et al., 2007) as the cratonic peridotites from the WG-NAC, the Kaapvaal and Slave craton. The simplest explanation for this striking observation is that after sulphides are removed from a residue, alloys with very low  $[Pd/Ir]_N$  stabilize and dominate the PGE

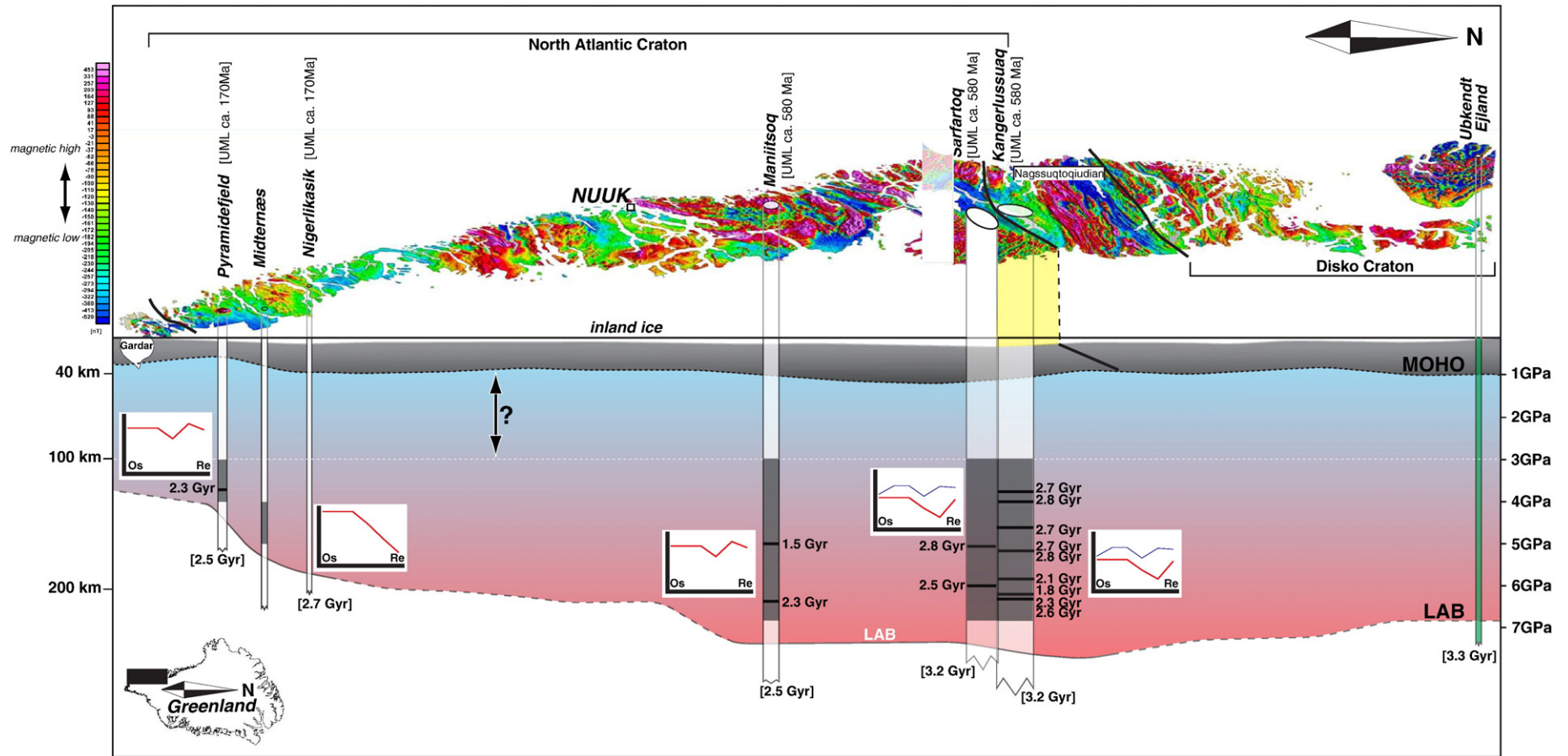


**Fig. 9.** Schematic cross section across the North Atlantic Craton and the Nagssugtoquidian mobile belt towards Ubekendt Eijland on the Disko Craton showing the total field magnetic profile (in nanotesla) of the continental crust (Jensen et al., 2003) and the estimated depth and sampling range (dark grey) of the lithospheric mantle (Bizzarro and Stevenson, 2003; Nielsen et al., 2008; Sand et al., 2009) combined with  $T_{RD}^{UPt}$  model ages for selected samples and predominant PGE patterns (this study) at specific UML dykes (Pyramidefjeld, Nigerlikasik, Maniitsoq, Sarfartoq, Kangerlussuaq). Maximum  $T_{RD}^{UPt}$  Os model ages derived from xenoliths sampled at individual dykes are given in brackets. Also shown is the xenolith locality on Ubekendt Eijland (Bernstein et al., 2006a,b).

budget of cratonic melting residues, despite them comprising only a minute, possibly sub-per mille fraction of the modal mineralogy in these ultra-refractory peridotites. This has been confirmed by the recent discovery of Pt-rich and I-PGE-rich micro-alloys in depleted peridotites (Luguet et al., 2007). Overall, it is clear that the low  $[Pd/Ir]_N$  of many of the WG-NAC peridotites are consistent with the very high degrees of melting indicated from other depletion indices and with melting progressing well beyond sulphide extraction. The PGE behaviour at extremely high degrees of depletion is not well explored experimentally but data available from Archean SCLM suggests that depletion of PGEs continues past sulphide exhaustion and that fractionated, low  $[Pd/Ir]_N$  ratios are preserved and even enhanced during the continued melting. As such, we propose that PGE systematics in the majority of northern WG-NAC peridotites, including the low I-PGE abundances, result from I-PGE-rich alloy stabilization during the course of extreme melt extraction.

### 5.3. The timing of formation of the WG-NAC continental mantle roots

#### 5.3.1. $T_{RD}$ and $T_{Ma}$ model ages in whole-rock WG-NAC peridotites

Re–Os isotope data can be used to investigate the timing of mantle depletion events in two principle ways (Rudnick and Walker, 2009 and references therein). First, Re–Os isotopes may be used in the traditional isochron approach, assuming the Re–Os isotopes were “set” with a melting event and subsequently evolve undisturbed to the present-day. As a consequence  $^{187}Re/^{187}Os$  and  $^{187}Os/^{187}Os$  should become tightly correlated in undisturbed peridotites. The WG-NAC peridotites do not show such an isochronous correlation (Fig. 6 and supplementary data file Fig. D) nor do  $T_{RD}^{erupt}$  ages correlate with Al contents (Fig. 2) which, in many instances, has been used to estimate the age of lithospheric mantle (alumachron, e.g., Reisberg and Lorand, 1995). This scattered relationship between  $^{187}Os/^{188}Os$  and Al is the norm for cratonic peridotite xenoliths (Pearson et al., 2004).

An alternative approach to iso- and alumachrons is to calculate Re–Os model ages. Here, at least three types of Os model ages are distinguished. In its simplest form, the Os model age ( $T_{Ma}$ ) uses Re–Os isotope systematics modelled back in time relative to a reference mantle evolution trend and is equivalent to Nd and Hf model ages (Walker et al., 1989). Clearly, a single-stage process affecting both Re and Os abundances and isotope data is a requirement for the use of  $T_{Ma}$  model ages. Considering the obvious Re enrichment relative to the PGEs shown in the (Figs. 5, 8, and 10) extended PGE plots, and the lack of an isochronous relationship in WG-NAC peridotites, the assumption that  $^{187}Re/^{187}Os$  systematics remain robust seems unlikely. Alternatively, “Rhenium depletion” model ages ( $T_{RD}$ ) assume that Re measured in peridotites is entirely of metasomatic origin; a valid proposition given the incompatibility of Re and the likelihood that at >30% melting, indicated from major elements, all Re would be removed from the initial residues of melting. As a consequence, the  $T_{RD}$  model age was developed, which assumes that Re/Os ratios were reduced to 0 at the time of melt depletion (Walker et al., 1989). The evidence for this later enrichment comes from the pronounced Re enrichment seen in the extended PGE patterns (Pearson et al., 2004, Fig. 5). These  $T_{RD}$  model ages consequently do not rely on the ingrowth of Os isotopes from the decay of  $^{187}Re$ , and they instead yield minimum model ages. A slight variation to the  $T_{RD}$  model ages are  $T_{RD}^{erupt}$  model ages, which assumes that the Re measured was introduced at the time of eruption of the host volcanic rocks of mantle xenoliths (Pearson et al., 1995).  $T_{RD}^{erupt}$  model ages are thus calculated in two steps, the period after eruption with the measured Re/Os ratios and the period prior to eruption with Re/Os of 0 (for further information see supplementary data file).

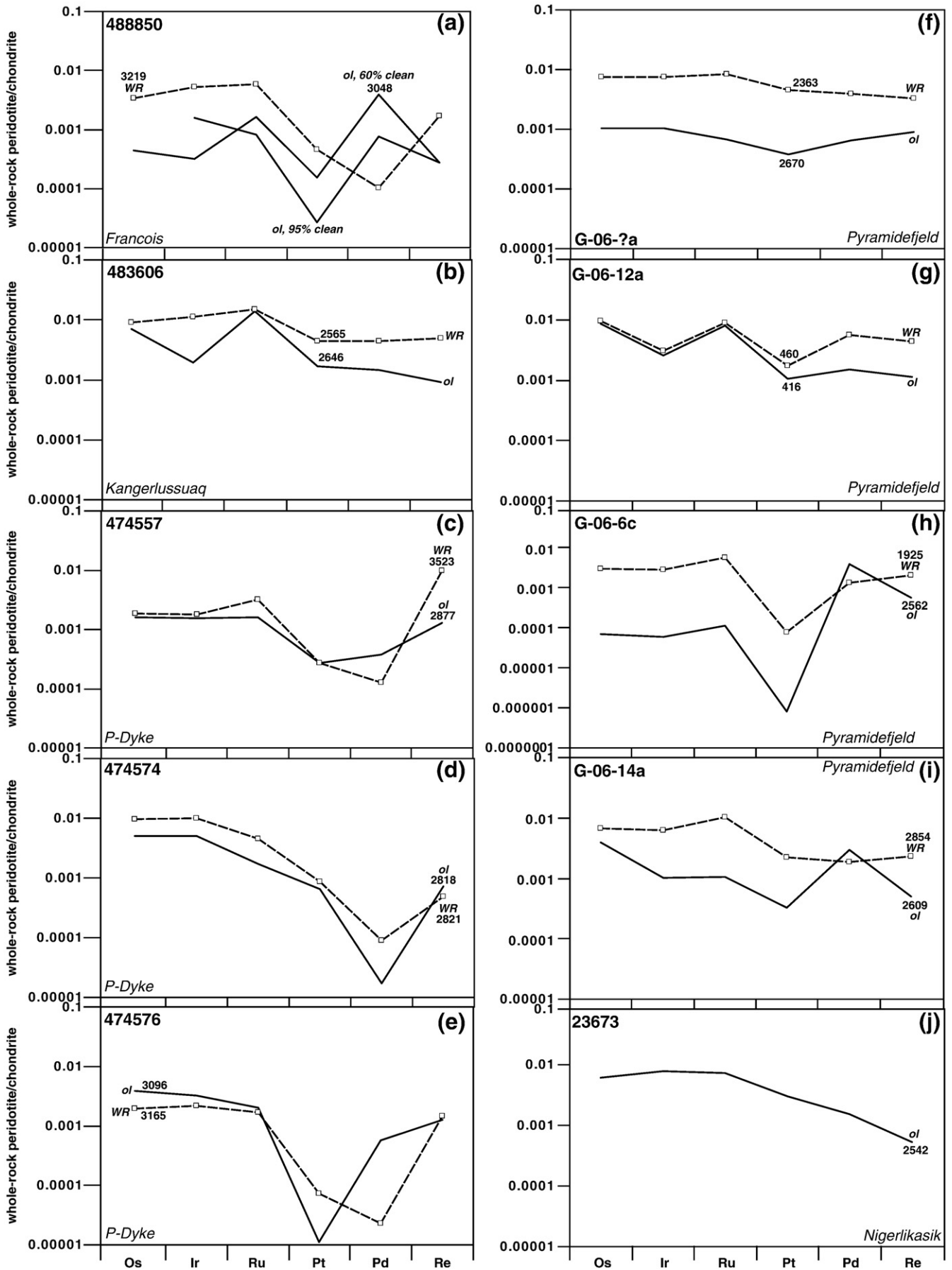
Having established the limitations of different dating approaches it may be appropriate to examine the validity of analysing whole-rock peridotites in the light of emerging sulphide Os isotope data (Alard et al., 2002; Griffin et al., 2004; Pearson et al., 2002). As outlined in

Section 5.2, we anticipate the complete to near-complete exhaustion of the sulphide fraction in cratonic SCLM. Any sulphide-bearing samples will, by definition, have acquired secondary sulphides and hence the PGE and Os isotope systematics predominantly record metasomatism rather than initial depletion. Consequently, focussing our study on sulphide-rich samples from the WG-NAC will yield a skewed picture of the PGE systematics. Furthermore, petrographic study of highly depleted cratonic peridotites with very low P-PGE abundances leads us to conclude that sulphides are generally scarce or even absent in these rocks. In some depleted orogenic peridotites, very rare PGE alloy grains were found but these are too small for accurate isotopic analyses and their discovery is extremely time consuming (Luguet et al., 2007). As such, our approach is to use combined whole-rock PGE data, in concert with Os isotope ratios, to make judgements about the likely degree of metasomatic disturbance in these peridotites (Pearson et al., 2004).

The WG-NAC peridotites, unsurprisingly, yield a substantial number of  $T_{Ma}$  model ages that are older than the earliest solids in the solar system (e.g., Baker et al., 2005) or Earth (16%, Fig. 7) or result in future ages (15%, not shown). This means that a third of the samples investigated here do not provide realistic  $T_{Ma}$  mantle melting ages (Fig. 7). Os isotope data acquired by laser ablation measurements of sulphides in peridotites typically lack precise Re/Os data, and also yield a high proportion of samples with extremely scattered and unrealistic  $T_{Ma}$  mantle melting ages that range from future ages to those exceeding the age of the Earth (Griffin et al., 2002).  $T_{RD}^{erupt}$  model ages of the WG-NAC peridotites that have unrealistic  $T_{Ma}$  only yield two samples with ages older than the solar system. It also has to be noted that all samples with  $T_{RD}^{erupt} > 2.8$  Gyr have unrealistic  $T_{Ma}$  model ages, which illustrates the sensitivity of ancient SCLM to the effects of Re addition. This observation also suggests that some portion of the measured Re might have been introduced prior to the eruption of the host volcanic rocks. Overall, the possible underestimation of  $T_{RD}^{erupt}$  model ages appears less problematic compared with the unrealistic ages derived by the  $T_{Ma}$  method for a large number of samples. Consequently, we prefer using  $T_{RD}^{erupt}$  model ages of whole-rock peridotites and will examine the age of the WG-NAC using this tool.

#### 5.3.2. The age of WG-NAC sub-continental lithospheric mantle

Earlier Os isotope studies from two xenolith localities in East and North-Western Greenland which, assuming the current definition of the NAC (Fig. 1), sample the continental mantle roots beneath the young Tertiary flood basalt province and the Disko Craton (Fig. 1), respectively, have revealed isotopically diverse, but generally old continental mantle roots beneath the continental crust of their respective regions (Fig. 1). In both cases, olivine and spinel separates were sampled from relatively low numbers of small sized xenoliths, from which it was impractical to make representative whole rocks. The  $^{187}Os/^{188}Os$  range in these samples is from 0.101 to 0.123 (Hanghøj et al., 2001) in East Greenland and 0.106 to 0.133 for Ubekendt Ejland (Bernstein et al., 2006a). These Os isotope systematics yield equally diverse  $T_{RD}$  model ages ranging from Paleoproterozoic in individual samples to future ages and there is no statistically relevant mode in Os isotopes (see supplementary data file Fig. E). A third occurrence of Greenlandic peridotites are the orogenic peridotites from the Central WG-NAC (Bennett et al., 2002), which are exposed in the Itsaq region (Fig. 1). These samples appear to have been uplifted into the earliest continental crust during the Eoarchean, presumably, in a subduction zone environment (Bennett et al., 2002; Friend et al., 2002). These samples have very unradiogenic Os isotopes in general, although radiogenic Os isotope ratios do occur (see supplementary data file Fig. E). It is not possible to estimate the thickness of the lithosphere at the time of emplacement of the orogenic peridotites, but the event is unlikely to have been one of the stable cratonic nuclei. In comparison to the available Os isotope data



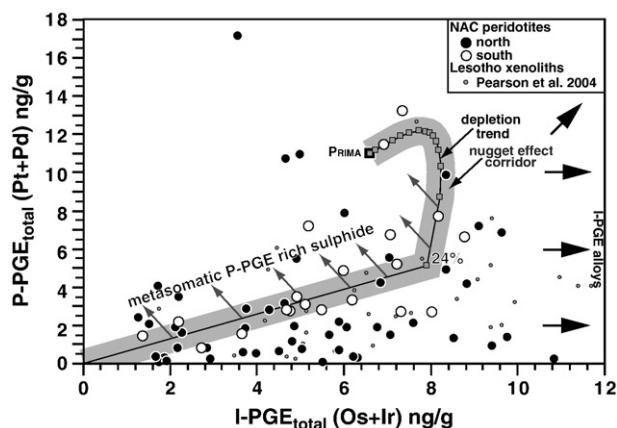


**Fig. 11.** Total P-PGE versus total I-PGE in ng/g of northern and southern WG-NAC whole-rock peridotites. The melt depletion evolution of primitive mantle is shown in 1% increments. Depletion in excess of 24% is extrapolated to zero (dashed line, grey band is following the northern WG-NAC samples). Also shown is the anticipated effect of introduction of interstitial metasomatic P-PGE-rich sulphides and the stabilization of I-PGE-rich alloys. For comparison, data from Lesotho whole-rock peridotites is shown (Pearson et al., 2004).

from East Greenland, Ubekendt Ejland and Central WG-NAC, our Re–Os data provide a clearer picture of the prevailing Os isotope composition of the SCLM of SW Greenland (Figs. 2 and 7).

We have outlined earlier that the WG-NAC continental crust is dominated by units with U–Pb zircon ages ranging between 2.8 and 3.2 Gyr and that a number of terranes in the central WG-NAC yield ages that are older than 3.5 Gyr (Nutman et al., 2004, Fig. 2). We recognize two relevant peaks in the  $T_{RD}^{RuPt}$  model ages, one between ca. 2.7 Gyr and 3.2 and a second at ca. 2.0 Gyr. The older age cluster is only present in samples from the northern margin of the WG-NAC, and importantly, in the reworked Archean of the Nagssugtoqidian belt. These samples are all marked by very low P-PGE abundances indicating extreme depletion in the Archean. The abundances of these samples in the SCLM beneath the Nagssugtoqidian belt clearly indicates that Archean SCLM extends northward beneath the Nagssugtoqidian continental crust as proposed by van Gool et al. (2002) from structural considerations.

Although the major formation episode of continental crust and the  $T_{RD}$  age peak for the supporting lithospheric mantle beneath SW Greenland agree exceptionally well and point to lithosphere stabilization between 2.7 and 3.2 Gyr, the currently available Re–Os isotope data from the WG-NAC xenoliths is clearly devoid of Eoarchean  $T_{RD}^{RuPt}$  model ages. The very old crustal ages have been documented from several terranes and also from the orogenic peridotites that are all located in the centre of the WG-NAC (Figs. 1 and 2). Obviously, the lack of Eoarchean Os isotope ages from peridotites in our study may be due to the lack of xenolith sampling sites directly beneath these Eoarchean terranes. Further mapping and sampling efforts in Greenland may reveal additional xenolith–kimberlite sites in these central parts of Greenland. However, we note that preliminary Re–Os isotope analyses of relatively fertile xenoliths from our most central sampling locality Maniitsoq has revealed peridotites with relatively radiogenic Os and therefore seemingly Paleoproterozoic SCLM ( $T_{RD}^{RuPt}$  model ages 1.5 to 2.5 Gyr).

In order to further investigate the lack of Eoarchean Re–Os isotope systematics in the WG-NAC xenolith record, we also analysed olivine separates from selected northern and southern WG-NAC peridotites.

We assume that these silicate minerals, at least partially, result from the melting process and precipitated during melt depletion, as a result of the consumption of clinopyroxene, orthopyroxene and spinel (Walter, 2003). These olivines may host sulphide and alloy inclusions that became associated with each other during the depletion process (Lorand and Gregoire, 2006). Such inclusions may have been shielded from passing metasomatic fluids and thus may preserve an older, more pristine Os isotope and PGE record than the associated whole-rock peridotites. However, it appears that most olivine separates from the northern region have somewhat elevated Pd abundances relative to their Pt, and also the Pd of their host rocks. Their  $T_{RD}^{RuPt}$  model ages are typically slightly younger than the corresponding Pd-depleted whole rocks (e.g., 488850, 474557, and 474646, Fig. 10) and converge towards 2.8 Gyr (Fig. 2). Overall, these olivines have Re–Os isotope systematics that are reasonably close to those of the corresponding whole rocks and do not preserve evidence of Eoarchean depletion (Fig. 10).

The only Paleoproterozoic  $T_{RD}^{RuPt}$  model age from the northern WG-NAC (474557, 3.5 Gyr  $T_{RD}^{RuPt}$ ) cannot be verified from the corresponding olivine Re–Os isotope systematics, which suggests that there may have been post-eruption addition of Re to the whole rock such that the  $T_{RD}^{RuPt}$  approach over-corrects for radiogenic Os in-grown since eruption. For this sample the 2.9 Gyr  $T_{RD}$  model age of the olivine separate may be closer to the melting age.

In addition to the prominent  $T_{RD}$  peak between ca. 2.7 and 3.2 Gyr, Re depletion ages in peridotites from the southern WG-NAC and a subset of the northern WG-NAC whole-rock peridotites cluster between 2.3 and 2.6 Gyr and at ca. 2.0 Gyr (Figs. 2, 4 and 7). Whereas there is no magmatic event that can be associated with the 2.3 to 2.6 cluster, granulite-facies metamorphism is thought to have occurred during this time (Bridgwater et al., 1973). Such high grade metamorphism must have resulted from a large thermal spike in the base of the crust.

Between 1.8 and 2.0 Gyr, the Nagssugtoqidian mobile belt became active and the Kangâmiut Dyke swarm was emplaced in the WG-NAC (Figs. 2, 4, 7). The group of samples with ca. 2.0 Gyr  $T_{RD}^{RuPt}$  model ages show P-PGE depletion, consistent with their origin as melt residues, indicating that new lithospheric mantle was added at 2.0 Gyr (e.g., 488866, P-Dyke b, 474527, 474555, 474577 and Maniitsoq samples). In contrast to these melt depletion signatures, Pd enrichment is present in other samples suggesting precipitation of secondary sulphides possibly as a result of the percolation of the Kangâmiut Dyke magmas through the lithosphere (e.g., 474570, 488858, 474575, see next section). Overall, the peridotites from the southern margin of the WG-NAC lack the Mesoarchean Os isotope signatures of the northern WG-NAC, while their corresponding olivines typically yield older, Archean  $T_{RD}^{RuPt}$  model ages compared with the whole-rock Re–Os isotope systematics.

Finally, it is also apparent that the circa 1.2 Ga Neoproterozoic magmatic activity (Larsen and Rex, 1992, carbonatites and kimberlites) in this region has not left a perceptible imprint on the Re–Os isotope systematics of the SCLM, although Hf–Nd isotope data from garnet and clinopyroxenes of these peridotites clearly shows the imprint of the host volcanic rocks (Wittig et al., 2008b) on the lithophile element record. Overall, we recognize a global peak in  $T_{RD}$  model ages between ca. 2.7 and 3.2 Gyr when cratonic lithospheric mantle is considered, which coincides with the most significant peak derived from zircons from continental crust (Condie, 1998), including that from the WG-NAC (Fig. 12, Pearson and Wittig, 2008). This provides further evidence for the linkage between the production of continental crust and the stabilization of the supporting continental mantle roots in Archean subduction zones (Pearson et al., 2007).

**Fig. 10.** Chondrite-normalized PGE patterns of olivine-whole-rock pairs from the northern (a–e) and southern (f–i) WG-NAC in addition to one olivine separate from Nigerliikasik (j) from the southern WG-NAC. Overall, olivines have lower Os, Ir and Pt abundances than the corresponding whole rocks and Pd appears to be enriched compared to the remaining PGEs and the whole rocks. Also given are the  $T_{RD}^{RuPt}$  Os model ages in Myr (e.g., 3219). Note that olivine separates from the northern WG-NAC with relatively high Pd have  $T_{RD}^{RuPt}$  Os model ages slightly younger than their whole rocks. Chondrite after McDonough and Sun (1995).

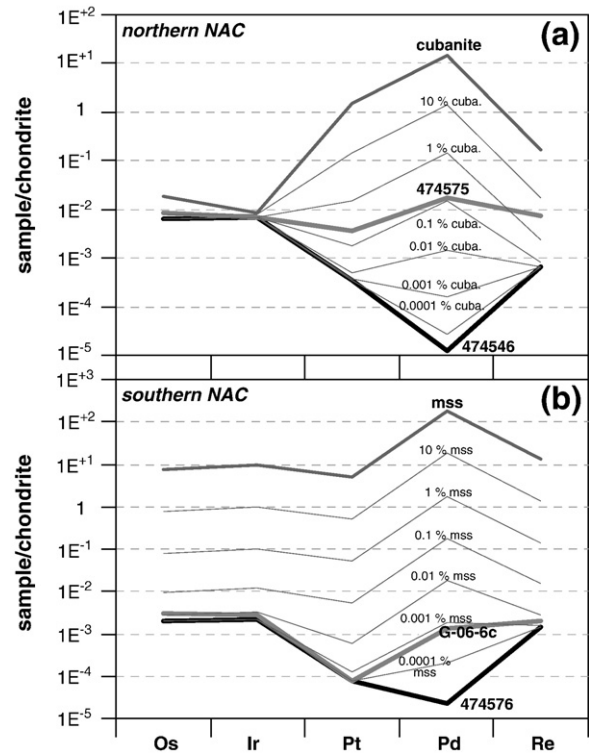
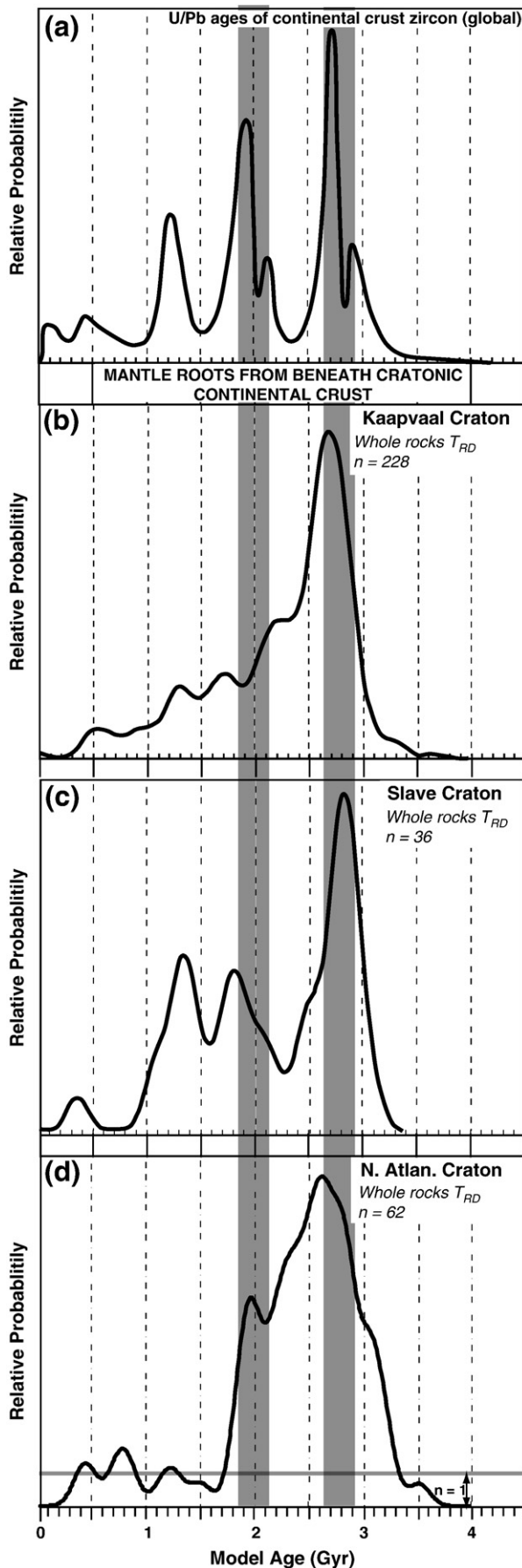


**Fig. 13.** Chondrite-normalized PGE patterns showing the effects of sulphide introduction into an I-PGE alloy dominated peridotite residue. We use samples with the lowest Pd abundances from the northern WG-NAC (474546, (a), 474576 (b)) as proxy for highly depleted mantle residues and introduce fractions of cubanite (a) and monosulphide solution (b, mss) in order to mimic metasomatic enrichment due to sulphide precipitation. The PGE systematics of two samples with non-depleted Pd abundances (474575, (a); G-06-6c (b)) can be reproduced by introducing 0.1% cubanite and 0.001% mss, respectively into the Pd-depleted peridotites. Cubanite and mss were taken from Barnes et al. (2006). Exact mixing fractions depend on sulphide composition, however, this simple model illustrates the sensitivity of highly depleted peridotites to sulphide precipitation from passing melts. More importantly, this numerical modelling approach highlights the refractory and overall unmetasomatized nature of the majority of the northern WG-NAC peridotites, whereas the peridotites from the southern margin of the WG-NAC record P-PGE enrichment possibly due to the precipitation of magmatic sulphides.

#### 5.4. Secondary alteration of siderophile elements in WG-NAC continental mantle roots

We have established that the majority of samples from the northern region of the WG-NAC, and also the SCLM from beneath the adjacent Nagssuqtoqidian mobile belt are marked by Archean  $T_{RD}^{rupt}$  Os model ages and show P-PGE depletion, consistent with extreme melt extraction as predicted by the depletion models (Bockrath et al., 2004; Pearson et al., 2004, Fig. 5). However, an important portion of samples from the north and nearly all southern peridotites show pronounced Pd enrichment (Fig. 8), relatively high  $[Pd/Ir]_N$  (Figs. 4, 5, and 7) and also comparatively radiogenic Os isotopes that give  $T_{RD}^{rupt}$  Os model ages  $\leq 2.0$  Gyr (Figs. 2, 4, and 7). Furthermore, this fraction of the peridotites has elevated FeO abundances (Wittig et al., 2008a, Fig. 2), which appear to be coupled to high Pd and  $[Pd/Ir]_N$  (Fig. 4 and supplementary data Fig. C). Although this FeO enrichment is not correlated with whole-rock major or lithophile trace element contents it appears that elevated FeO is predominantly found in peridotites with  $T_{RD}^{rupt}$  model ages between

**Fig. 12.** Density probability plots comparing the currently available U/Pb ages of zircons from the continental crust (a) with  $T_{RD}$  Os model ages from the continental mantle peridotites from the Kaapvaal (b), Slave (c) and North Atlantic Craton (d, this study). Note the strong mode of formation and depletion ages between 2.6 and 2.9 Gyr in the continental crust and their mantle roots. After Condie (1998) and Pearson and Wittig (2008) and references therein.

2.3 and 2.6 and ages younger than 0.9 Gyr. As noted above, granulite-facies metamorphism occurred during this time (Bridgwater et al., 1973), but considering the spread in ages present, it seems more likely that these ages are simple mixtures.

In contrast to the disturbed high FeO samples (Fig. 2), the majority of northern WG-NAC peridotites with Archean  $T_{RD}^{FePt}$  model ages have lower FeO (and also Pd) contents, in agreement with a shallow 2 to 3 GPa melting regime suggested for these and other cratonic peridotites (Canil, 2002, 2004; Wittig et al., 2008a). Similarly, peridotites from both the southern and northern WG-NAC with  $T_{RD}^{FePt}$  model ages clustering around 2.0 Gyr have low FeO abundances that are also consistent with a residual origin during a lithosphere building event (Fig. 2). These relations correlate the main, depleted peridotite suite with the 2 major recognisable crust generation events while a minority, with elevated FeO abundances, show clear evidence of PGE metasomatism (Fig. 2). Wittig et al. (2008a) suggested that ultramafic melts (i. e., komatiites) may be responsible for this selective FeO enrichment based on the fact that reaction between komatiites and refractory peridotites would not necessarily alter major elements such as MgO or  $Al_2O_3$  but may cause high FeO (>9 wt.%) in these peridotites.

It is interesting to consider what the effects of infiltrating ultramafic melts into the WG-NAC lithosphere might have been. Ultramafic to mafic silicate melts show diverse PGE patterns, although typically these are marked by higher P-PGE abundances relative to I-PGEs (e.g., Bockrath et al., 2004; Dale et al., 2008; Puchtel and Humayun, 2000; Rehkämper et al., 1999). The introduction of magmatic sulphides back into the mineral matrix of residual peridotites will likely result in elevated P-PGEs in such metasomatised peridotites. Consequently, metasomatised peridotites are anticipated to have variable I-PGE abundances and elevated P-PGEs relative to our modelled residual mantle. Fig. 13 illustrates the effect of assimilating magmatic sulphides into the mineral matrix of highly depleted peridotites using two examples. We use the most depleted peridotites from the northern NAC (474546 and 474576) and mix these with fractions of magmatic sulphides. The PGE patterns of representative metasomatic samples from the northern NAC (474575) and the south (G-06-6c) can be reproduced if the residual patterns of 474546 and 474576 are mixed with 0.1% and 0.001% fractions of cubanite and monosulphide solution taken from Barnes et al. (2006), respectively. Clearly, the individual mixing relationships of residue and different types of sulphides are variable and traditionally Cu-rich sulphides are anticipated to present as metasomatic phases (e.g. Luguët et al., 2001, 2003; Lorand et al., 2008); however, the WG-NAC peridotites have low Cu abundances that do not systematically correlate with PGEs. With our very simple modelling approach we wish to illustrate how strongly an ultra-depleted mantle residue will respond to minute levels of newly precipitated sulphides. At the same time, this model highlights that such modal sulphide enrichment is of little relevance in the peridotites of the northern WG-NAC and in fact most Archean SCLM studied thus far, while the samples from the southern WG-NAC typically have PGE systematics that appear to require the precipitation of metasomatic sulphides (Fig. 5), as shown by some sulphide-enriched peridotites (Alard et al., 2002). It seems plausible that the percolation of Mg-rich mafic silicate melts may have resulted in elevated FeO and Pd abundances that are now present in a fraction of WG-NAC peridotites.

## 6. Conclusion and implications for diamond potential

PGE abundance and Re–Os isotope data for peridotites from southwest Greenland reveal important insights into the timing of the stabilization of the North Atlantic Craton continental mantle root and the age structure of the SCLM beneath the Nagssugtoqidian mobile belt.

- (1) The whole-rock peridotites from the northern and southern WG-NAC have substantially different PGE systematics, Os isotopes

and hence  $T_{RD}^{FePt}$  model ages. While the southern WG-NAC SCLM appears to have experienced substantial metasomatic alteration of their PGE budgets yielding mainly Proterozoic  $T_{RD}^{FePt}$  model ages, the northern WG-NAC lithosphere preserves extreme Pd and Pt depletion, unradiogenic Os isotopes and Neo- to Mesoproterozoic  $T_{RD}^{FePt}$  model ages. These features are typical of cratonic SCLM peridotites in general.

- (2) The northern WG-NAC peridotites have  $T_{RD}^{FePt}$  model ages that cluster between 2.8 and 3.2 Gyr even for samples erupted through the crust that comprises the Nagssugtoqidian suture zone. The WG-NAC-Nagssugtoqidian suture seems to be a shallow structure and the SCLM beneath the Nagssugtoqidian mobile belt is generally Archean. This conclusion has clear implications for diamond exploration in this region. Sand et al. (2009) have shown that the lithosphere beneath that part of West Greenland extends well into the diamond stability field both on the craton and beneath the Nagssugtoqidian mobile belt in the areas we have sampled. We show here that this SCLM is Archean, making this part of the region equally prospective as the “on-craton” areas from these considerations alone.
- (3) The U–Pb zircon ages of the WG-NAC TTG and granite crust exhibit a very strong mode between 2.8 and 3.1 Gyr. We suggest that, in common with a number of other cratons, the main phase of lithospheric mantle formation took place in a late Archean subduction zone environment.
- (4) A small number of northern and the majority of southern WG-NAC peridotites have Re–Os isotope systematics resulting in  $T_{RD}^{ReOs}$  model ages of ca. 2.0 Gyr. The northern WG-NAC peridotites with 2.0 Gyr  $T_{RD}^{ReOs}$  model ages have PGE systematics indicative of both extreme mantle melting and PGE enrichment. The strong Paleoproterozoic peak in  $T_{RD}^{ReOs}$  model ages is reflected in the continental crust adjacent to the WG-NAC, which originated at ca. 1.8 Gyr, while initial rifting of the WG-NAC at 2.0 Gyr emplaced the extensive Kangâmiut dyke swarm.
- (5) A number of peridotites have  $T_{RD}^{FePt}$  model ages of between 2.3 and 2.6 Gyr and some of these samples have Pd and FeO abundances inconsistent with residual mantle. These samples appear to have been disturbed by the infiltration of ultramafic melts. Knowledge of the PGE and Os isotope data not only allows reconstruction of the timing of the stabilization of the WG-NAC, but may help in understanding elevated FeO abundances in peridotites.

## Acknowledgements

This study was supported by the Natural Environment Research Council (NERC, UK, NE/C5/9054/1). We kindly acknowledge support by De Nationale Geologiske Undersøgelser for Danmark og Grønland (GEUS), Air Greenland (2004, 2006) and the hospitality of the Grønlands Kommando in Grønneal during the field campaign in 2006. We thank Henry Emeleus for his map of Pyramidefjeld that was an invaluable source of xenoliths targets. L. Nielsen is thanked for good company around Pyramidefjeld and thanks to Sarah Porter for help with sample preparation. Sebastian Tappe is appreciated for (twice) reminding NW of the existence of the Labrador alkaline intrusives. We also thank an anonymous reviewer and Karen Hanghøj for their comments, which helped to improve the manuscript and Roberta Rudnick for editorial handling.

## Appendix A. Supplementary data

Supplementary data associated with this article can be found, in the online version, at doi:10.1016/j.chemgeo.2010.06.002.

## References

- Alard, O., Griffin, W.L., Pearson, N.J., Lorand, J.-P., O'Reilly, S.Y., 2002. New insights into the Re–Os systematics of sub-continental lithospheric mantle from in situ analysis of sulfides. *Earth Planet. Sci. Lett.* 203, 651–663.
- Andrews, J.R., Emeleus, C.H., 1975. Structural aspects of kimberlite dyke and sheet intrusion in South-West Greenland. *Phys. Chem. Earth* 9, 43–50.
- Aulbach, S., Griffin, W.L., Pearson, N.J., O'Reilly, S.Y., Doyle, B.J., 2007. Lithosphere formation in the Central Slave Craton (Canada): plume accretion or lithosphere accretion. *Contrib. Mineralog. Petrol.* 154, 409–428.
- Aulbach, S., Griffin, W.L., O'Reilly, S.Y., McCandless, T.E., 2004. Mantle formation and evolution, Slave craton: constraints from HSE abundances and Re–Os isotope systematics of sulfide inclusions in mantle xenocrysts. *Chem. Geol.* 208, 61–88.
- Baker, J.A., Bizzarro, M., Wittig, N., Connelly, J., Haack, H., 2005. Early planetesimal melting from an age of 4.5662 Gyr for differentiated meteorites. *Nature* 436, 1127–1131.
- Barnes, S.-J., Cox, R.A., Zientek, M.L., 2006. Platinum-group element, Gold, Silver, and Base Metal distribution in compositionally zone sulphide droplets from the Medvezky Creek Mine, Noril'sk, Russia. *Contrib. Mineralog. Petrol.* 152, 187–200.
- Bennett, V.C., Nutman, A.P., Esat, T.M., 2002. Constraints on mantle evolution from  $^{187}\text{Os}/^{188}\text{Os}$  isotopic compositions of Archean ultramafic rocks from southern West Greenland (3.8 Ga) and Western Australia (3.46 Ga). *Geochim. Cosmochim. Acta* 66, 2615–2630.
- Bernstein, S., Brooks, C.K., 1998. Mantle xenoliths from Tertiary lavas and dykes on Ubekend Ejlund, West Greenland. *Geol. Greenland Surv. Bull.* 180, 152–154.
- Bernstein, S., Kelemen, P.B., Brooks, C.K., 1998. Depleted spinel harzburgite xenoliths in Tertiary dykes from East Greenland: restites from high melting degrees. *Earth Planet. Sci. Lett.* 154, 221–235.
- Bernstein, S., Hanghøj, K., Kelemen, P.B., Brooks, C.K., 2006a. Ultra-depleted, shallow cratonic mantle beneath West Greenland: dunitic xenoliths from Ubekend Ejlund. *Contrib. Mineralog. Petrol.* 152, 335–347.
- Bernstein, S., Kelemen, P.B., Hanghøj, K., 2006b. Consistent olivine Mg# in cratonic mantle reflects Archean mantle melting to the exhaustion of orthopyroxene. *Geology* 35, 459–462.
- Bleeker, W., 2003. The late Archean record: a puzzle in ca. 35 pieces. *Lithos* 71, 99–134.
- Bizzarro, M., Stevenson, R.K., 2003. Major element composition of the lithospheric mantle under the North Atlantic craton: evidence from peridotite xenoliths of the Sarfartoq area, southwest Greenland. *Contrib. Mineralog. Petrol.* 146, 223–240.
- Bockrath, C., Ballhaus, C., Holzheid, A., 2004. Fractionation of the platinum-group elements during mantle melting. *Science* 305, 1951–1953.
- Boyd, F.R., 1989. Compositional distinction between oceanic and cratonic lithosphere. *Earth Planet. Sci. Lett.* 96, 15–26.
- Boyd, F.R., Nixon, P.H., 1975. Origins of ultramafic nodules from some kimberlites of northern Lesotho and the Monastery Mine, South Africa, Physics and Chemistry of the Earth. Academic Press, pp. 431–451.
- Bridgwater, D., Watson, J., Windley, B.F., 1973. The Archean craton of the North Atlantic region. *Philos. Trans. R. Soc. Lond.* 273, 493–512.
- Cabri, L.J., 2002. The platinum-group minerals. In: L.J. Cabri (Ed.), *The Geology, Geochemistry, Mineralogy and Mineral Beneficiation of Platinum-Group Elements*, Canadian Institute of Mining, Metallurgy and Petroleum, Special Volume 54, pp. 13–129.
- Canil, D., 2002. Vanadium in peridotites, mantle redox and tectonic environments: archean to present. *Earth Planet. Sci. Lett.* 195, 75–90.
- Canil, D., 2004. Mildly incompatible elements in peridotites and the origins of mantle lithosphere. *Lithos* 77 (1–4), 375–393.
- Carlson, R.W., Irving, A.J., 1994. Depletion and enrichment history of subcontinental lithospheric mantle: An Os, Sr, Nd and Pb isotopic study of ultramafic xenoliths from the northwestern Wyoming Craton. *Earth Planet. Sci. Lett.* 126, 457–472.
- Carlson, R.W., Moore, R.O., 2004. Age of the Eastern Kaapvaal mantle: Re–Os isotope data for peridotite xenoliths from the Monastery mine. *S. Afr. J. Geol.* 107, 81–90.
- Carlson, R.W., Irving, A.J., Schulze, D.J., Hearn, J., C., B., 2004. Timing of Precambrian melt depletion and Phanerozoic refertilization events in the lithospheric mantle of the Wyoming Craton and adjacent Central Plains Orogen. *Lithos* 77 (1–4), 453–472.
- Carlson, R.W., Pearson, D.G., James, D.E., 2005. Physical, chemical, and geochronological characteristics of continental mantle. *Rev. Geophys.* 43 (RG1001) 2004RG000156.
- Caro, G., Bourdon, B., Birck, J.L., Moorbath, S., 2003.  $^{146}\text{Sm}$ – $^{142}\text{Nd}$  evidence from Isua metamorphosed sediments for early differentiation of the Earth's mantle. *Nature* 423, 428–432.
- Chesley, J.T., Rudnick, R.L., Lee, C.-T., 1999. Re–Os systematics of mantle xenoliths from the East African Rift: age, structure, and history of the Tanzanian craton. *Geochim. Cosmochim. Acta* 63, 1203–1217.
- Chesley, J., Righter, K., Ruiz, J., 2004. Large-scale mantle metasomatism: a Re–Os perspective. *Earth Planet. Sci. Lett.* 219, 49–60.
- Condie, K.C., 1998. Episodic continental growth and supercontinents: a mantle avalanche connection. *Earth Planet. Sci. Lett.* 163, 97–108.
- Dale, C.W., Luguét, A., Macpherson, C.G., Pearson, D.G., Hickey-Vargas, 2008. Extreme platinum-group element fractionation and variable Os isotope compositions in Philippine Sea Plate basalts: tracing mantle source heterogeneity. *Chem. Geol.* 248, 213–238.
- Emeleus, C.H., Andrews, J.R., 1975. Mineralogy and petrology of kimberlite dyke and sheet intrusions and included peridotite xenoliths from South-West Greenland. *Phys. Chem. Earth* 9, 179–197.
- Frei, R., Rosing, M., 2001. The least radiogenic terrestrial leads: implications for the early Archean crustal evolution and hydrothermal–metasomatic processes in the Isua Supracrustal Belt (West Greenland). *Chem. Geol.* 181, 47–66.
- Friend, C.L., Bennett, V.C., Nutman, A.P., 2002. Abyssal peridotites >3, 800 Ma from southern West Greenland: field relationships, petrography, geochronology, whole-rock and mineral chemistry of dunite and harzburgite inclusions in the Itsaq Gneiss Complex. *Contrib. Mineralog. Petrol.* 143, 71–92.
- Gaffney, A.M., Blichert-Toft, J., Nelson, B.K., Bizzarro, M., Rosing, M., Albareda, F., 2007. Constraints on source-forming processes of West Greenland kimberlites inferred from Hf–Nd isotope systematics. *Geochim. Cosmochim. Acta* 71, 22–238.
- Gool, J.A.M.V., Connelly, J.N., Marker, M., Mengel, F.C., 2002. The Nagssugtoqidian Orogen of West Greenland: tectonic evolution and regional correlations from a West Greenland perspective. *Can. J. Earth Sci.* 39, 665–686.
- Griffin, W.L., Graham, S., O'Reilly, S.Y., Pearson, N.J., 2004. Lithosphere evolution beneath the Kaapvaal Craton: Re–Os systematics of sulfides in mantle-derived peridotites. *Chem. Geol.* 208, 195–215.
- Griffin, W.L., O'Reilly, S.Y., Ryan, C.G., 1999. The composition and origin of sub-continental lithospheric mantle. In: Fei, Y., Bertka, C.M., Mysen, B.O. (Eds.), *Mantle Petrology: Field observations and high pressure experimentation: A tribute to Francis R. (Joe) Boyd: The Geochemical Society, Special Publication*, pp. 13–45.
- Griffin, W.L., O'Reilly, S.Y., Pearson, N.J., Graham, S., 2002. In situ Re–Os dating of sulfides in Kaapvaal xenoliths. *Geochim. Cosmochim. Acta* 66 (S1), A292.
- Handler, M.R., Bennett, V.C., 1999. Behaviour of platinum-group elements in the subcontinental mantle of eastern Australia during variable metasomatism and melt depletion. *Geochim. Cosmochim. Acta* 63, 3597–3618.
- Hanghøj, K., Kelemen, P.B., Bernstein, S., Blustztajn, J., Frei, R., 2001. Osmium isotopes in the Wiedemann Fjord mantle xenoliths: a unique record of cratonic mantle formation by melt depletion in the Archean. *Geochem. Geophys. Geosyst.* 2 2000GC000085.
- Hart, S.R., Gaetani, G.A., 2006. Mantle Pb paradoxes: the sulfide solution. *Contrib. Mineralog. Petrol.* 152, 295–308.
- Heaman, L.M., 2005. Patterns of kimberlite emplacement—the importance of robust geochronology, Workshop on Greenland's diamond potential. *Danmarks og Grønlands Geologiske Undersøgelse Rapport 2005/68*, Copenhagen.
- Herzberg, C., 2004. Geodynamic information in peridotite petrology. *J. Petrol.* 45, 2507–2530.
- Hutchison, M., Frei, D., 2009. Kimberlite and related rocks from Garnet Lake, West Greenland, including their mantle constituents, diamond occurrence, age and provenance. *Lithos* 112, 318–333 Supplement 1.
- Irvine, G.J., Pearson, D.G., Carlson, R.W., 2001. Lithospheric mantle evolution in the Kaapvaal craton: a Re–Os isotope study of peridotite xenoliths from Lesotho kimberlites. *Geophys. Res. Lett.* 28, 2505–2508.
- Irvine, G.J., Pearson, D.G., Kjarsgaard, B.A., Carlson, R.W., Kopylova, M.G., Dreibus, G.E., 2003. A Re–Os isotope and PGE study of kimberlite-derived peridotite xenoliths from Somerset Island and a comparison to the Slave and Kaapvaal craton. *Lithos* 71, 461–488.
- Jensen, S.M., Lind, M., Rasmussen, T.M., S., F., Secher, K., 2003. Diamond exploration data from West Greenland a GIS and digital data compilation on DVD. *Danmarks og Grønlands Geologiske Undersøgelse Rapport 21((incl DVD))*. 2003. 1–50.
- Jensen, S.M., Secher, K., Rasmussen, T., 2004. Diamond content of three kimberlitic occurrences in southern West Greenland. *Danmarks og Grønlands Geologiske Undersøgelse Rapport* 19, 1–41.
- Larsen, L.M., 1991a. Occurrences of kimberlites, lamproites and ultramafic lamprophyry in Greenland. *Rapport Grønlands Geologiske Undersøgelse*, 91, p. 36. 2.
- Larsen, L.M., 1991b. Registration of kimberlites and other potentially diamond-bearing rocks in Greenland. *Rapp. Grøn. Geol. Unders.* 152, 61–65.
- Larsen, L.M., Rex, D.C., 1992. A review of the 2500 Ma span of alkaline ultramafic potassic and carbonatitic magmatism in West Greenland. *Lithos* 28, 367–402.
- Larsen, L.M., Ronsbo, J., 1993. Conditions of origin of kimberlites in West Greenland: new evidence from the Sarfartoq and Sukkertoppen regions. *Rapp. Grøn. Geol. Unders.* 159, 115–120.
- Lee, C.-T., 2006. Geochemical/petrological constraints on the origin of cratonic mantle. In: Benn, J.-C.M.K., Condie, K.C. (Eds.), *Archean geodynamics and environments: American Geophysical Union Monograph*, pp. 89–114.
- Lorand, J.-P., Alard, O., 2001. Platinum-group element abundances in the upper mantle: new constraints from in situ and whole-rock analyses of Massif Central xenoliths. *Geochim. Cosmochim. Acta* 65, 2789–2806.
- Lorand, J.-P., Gregoire, M., 2006. Petrogenesis of base metal sulphide assemblages of some peridotites from the Kaapvaal craton (South Africa). *Contrib. Mineralog. Petrol.* 151, 521–538.
- Lorand, J.-P., Reisberg, L., Bedini, R.M., 2003. Platinum-group elements and melt percolation in Sidamo spinel peridotite xenolith, Ethiopia, East African Rift. *Chem. Geol.* 196, 57–75.
- Lorand, J.-P., Luguét, A., Alard, A., 2008. Platinum-group elements: a new set of key tracers for the Earth's interior. *Elements* 4, 247–252.
- Luguét, A., Alard, O., Lorand, J.P., Pearson, N.J., Ryan, C.G., O'Reilly, S.Y., 2001. Laser-ablation microprobe (LAM)-ICP-MS unravels the highly siderophile element geochemistry of the oceanic mantle. *Earth Planet. Sci. Lett.* 189, 285–294.
- Luguét, A., Lorand, J.P., Seyler, M., 2003. Sulfide petrology and highly siderophile element geochemistry of abyssal peridotites: a coupled study of samples from the Kane Fracture Zone (45°W 23°20'N, MARK area, Atlantic Ocean), 67, pp. 1553–1570.
- Luguét, A., Shirey, S.B., Lorand, J.P., Horan, M.F., Carlson, R.W., 2007. Residual platinum-group minerals from highly depleted harzburgites of the Lherz massif (France) and

- their role in HSE fractionation of the mantle. *Geochim. Cosmochim. Acta* 71, 3082–3097.
- Luguet, A., Nowell, M., G., Pearson, D.G., 2008.  $^{184}\text{Os}/^{188}\text{Os}$  and  $^{186}\text{Os}/^{184}\text{Os}$  measurements by Negative Thermal Ionisation Mass Spectrometry (N-TIMS): effects of interfering element and mass fractionation corrections on data accuracy and precision. *Chem. Geol.* 248, 342–362.
- McDonough, W.F., Sun, S.S., 1995. The composition of the Earth. *Chem. Geol.* 120, 223–253.
- Meisel, T., Walker, R.J., Morgan, J.W., 1996. The osmium isotopic composition of the Earth's primitive upper mantle. *Nature* 383, 517–520.
- Menzies, M.A., Hawkesworth, C.J., 1987. Upper mantle processes and composition. In: Nixon, P.H. (Ed.), *Mantle Xenoliths*. John Wiley & Sons, New York, pp. 724–738.
- Nielsen, L.J., Hutchison, M.T., Malarkey, J., 2008. Geothermal constraints from kimberlite-hosted garnet lherzolites from southern Greenland, 9<sup>th</sup> International Kimberlite Conference, Frankfurt.
- Nutman, A.P., Friend, C.L., Barker, S.L.L., McGregor, V.R., 2004. Inventory and assessment of Palaeoarchean gneiss terrains and detrital zircons in southern West Greenland. *Precambrian Res.* 135, 281–314.
- Pearson, D.G., Woodland, S.J., 2000. Carius tube digestion and solvent extraction/ion exchange separation for the analysis of PGE's (Os, Ir, Pt, Pd, Ru) and Re–Os isotopes in geological samples by isotope dilution ICP–mass spectrometry. *Chem. Geol.* 165, 87–107.
- Pearson, D.G., Nowell, G.M., 2004. Re–Os and Lu–Hf isotopes constraints on the origin and age of pyroxenites from the Beni Bousera peridotite massif: implications for mixed peridotite–pyroxenite mantle sources. *J. Petrol.* 45 (2), 439–455.
- Pearson, D.G., Wittig, N., 2008. Formation of Archaean continental lithosphere and its diamonds: The root of the problem. *J. Geol. Soc.* 165, 895–914.
- Pearson, D.G., Carlson, R.W., Shirey, S.B., Boyd, F.R., Nixon, P.H., 1995. Stabilisation of Archaean lithospheric mantle: a Re–Os isotope study of peridotite xenoliths from the Kaapvaal Craton. *Earth Planet. Sci. Lett.* 134, 341–357.
- Pearson, D.G., Canil, D., Shirey, S.B., 2003. Mantle samples included in volcanic rocks: xenoliths and diamonds. In: Holland, H.D., Turekian, K.K. (Eds.), *Treatise on geochemistry*. Elsevier, Amsterdam, pp. 171–275.
- Pearson, D.G., Irvine, G.J., Ionov, D.A., Boyd, F.R., Dreibus, G.E., 2004. Re–Os isotope systematics and platinum group element fractionation during mantle melt extraction: a study of massif and xenolith peridotite suites. *Chem. Geol.* 208, 29–59.
- Pearson, D.G., Parman, S.W., Nowell, G.M., 2007. A link between large mantle melting events and continent growth seen in osmium isotopes. *Nature* 449, 202–205.
- Pearson, N.J., Alard, O., Griffin, W.L., Jackson, S.E., O'Reilly, S., 2002. In situ measurement of Re–Os isotopes in mantle sulfides by laser ablation multicollector inductively coupled plasma mass spectrometry: analytical methods and preliminary results. *Geochim. Cosmochim. Acta* 66, 1037–1050.
- Polat, A., Frei, R., 2005. The origin of early Archaean banded iron formations and of continental crust, Isua, southern West Greenland. *Precambrian Res.* 138 (1–2), 151–175.
- Polat, A., Hofmann, A.W., Münker, C., Regelous, M., Appel, P.W.U., 2003. Contrasting geochemical pattern in the 3.7–3.8 Ga pillow basalt cores and rims, Isua greenstone belt, Southwest Greenland: implications for postmagmatic alteration processes. *Geochim. Cosmochim. Acta* 67 (3), 441–457.
- Polat, A., Hofmann, A.W., Rosing, M.T., 2002. Boninite-like volcanic rocks in the 3.7 Ga Isua greenstone belt, West Greenland: geochemical evidence for intra-oceanic subduction zone processes in the early Earth. *Chem. Geol.* 184, 231–254.
- Puchtel, I., Humayun, M., 2000. Platinum group elements in Kstomuksha komatiites and basalts: implications for oceanic crust recycling and core–mantle interaction. *Geochim. Cosmochim. Acta* 64, 4227–4242.
- Rehkämper, M., Halliday, A.N., Fitton, J.G., Lee, D.C., Wieneke, M., Arndt, N.T., 1999. Ir, Ru, Pt and Pd in basalts and komatiites: new constraints for the geochemical behaviour of the platinum-group elements in the mantle. *Geochim. Cosmochim. Acta* 63, 3915–3934.
- Reisberg, L., Lorand, J.P., 1995. Longevity of sub-continental mantle lithosphere from osmium isotope systematics in orogenic peridotite massifs. *Nature* 376, 159–162.
- Rosing, M., Nutman, A.P., Loeffquist, L., 2001. A new fragment of the early earth crust: the Aasivik terrane of West Greenland. *Precambrian Res.* 105, 115–128.
- Rudnick, R.L., Walker, R.J., 2009. Interpreting ages from Re–Os isotopes in peridotites. *Lithos* 112, 1083–1095 Supplement 2.
- Sand, K.K., Waight, T.E., Pearson, D.G., Nielsen, T.R.D., Makovicky, E., Hutchison, M.T., 2009. The lithospheric mantle below southern West Greenland: a geothermobarometric approach to diamond potential and mantle stratigraphy. *Lithos*. doi:10.1016/j.lithos.2009.05.012.
- Schmidberger, S.S., Simonetti, A., Francis, D., Gariépy, C., 2002. Probing archaean lithosphere using Lu–Hf isotope systematics of peridotite xenolith from Somerset Island kimberlites, Canada. *Earth Planetary Sci.* 197, 245–259.
- Secher, K., et al., 2009. Timing of kimberlite, carbonatite and ultramafic lamprophyre emplacement in the alkaline province located 64–67 N in southern West Greenland. *Lithos* 400–406 Supplement 1.
- Shaw, J.E., Baker, J.A., Kent, A.J.R., Ibrahim, K.M., Menzies, M.A., 2007. Chemical and isotopic character of Arabian lithospheric mantle—a source for intraplate volcanism? *J. Petrol.* 48, 1495–1512.
- Shi, R., Alard, O., Zhi, X., O'Reilly, S.Y., Pearson, N., Griffin, W.L., Zhang, M., Chen, X., 2007. Multiple events in the Neo-Tethyan oceanic upper mantle: Evidence from Ru–Os–Ir alloys in the Luobusa and Dongqiao ophiolitic podiform chromitites, Tibet. *Earth Planet. Sci. Lett.* 261, 33–48.
- Simon, N., Carlson, R.W., Pearson, D.G., Davies, G.R., 2007. The origin and evolution of the Kaapvaal Cratonic lithospheric mantle. *J. Petrol.* 48, 589–625.
- Steenfelt, A., Garde, A.A., Møyn, J.-F., 2005. Mantle wedge involvement in the petrogenesis of Archaean grey gneisses in West Greenland. *Lithos* 79, 207–228.
- Tachibana, Y., Kaneoka, I., Gaffney, A.M., Upton, B.G.J., 2006. Ocean-island basalt-like source of kimberlite magmas from West Greenland revealed by high  $^3\text{He}/^4\text{He}$  ratios. *Geology* 34, 273–276.
- Tappe, S., Foley, S.F., Stracke, A., Romer, R.L., Kjarsgaard, B.A., Heaman, L.M., Joyce, N., 2007. Craton reactivation on the Labrador Sea margins: 40Ar/39Ar age and Sr–Nd–Hf–Pb isotope constraints from alkaline and carbonatite intrusives. *Earth Planet. Sci. Lett.* 256, 433–454.
- Walker, R.J., Carlson, R.W., Shirey, S.B., Boyd, F.R., 1989. Os, Sr, Nd, and Pb isotope systematics of southern African peridotite xenoliths: implications for the chemical evolution of subcontinental mantle. *Geochim. Cosmochim. Acta* 53, 1583–1595.
- Walter, M.J., 2003. Melt extraction and compositional variability in mantle lithosphere. In: Holland, H.D., Turekian, K.K. (Eds.), *Treatise on Geochemistry*. Elsevier.
- Webb, M., 2007. Re–Os isotope constraints on the age of the lithospheric mantle beneath Western Greenland. Durham University, Durham. 140 pp.
- Whitehouse, M.J., Kalsbeek, F., Nutman, A.P., 1998. Crustal growth and crustal recycling in the Nagssugtoqidian orogen of West Greenland: constraints from radiogenic isotope systematics and U–Pb zircon geochronology. *Precambrian Res.* 91, 365–381.
- Wittig, N., Baker, J.A., Downes, H., 2006. Dating the mantle roots of young continental crust. *Geology* 34 (4), 237–240.
- Wittig, N., Baker, J.A., Downes, H., 2007. U–Th–Pb and Lu–Hf isotopic constraints on the evolution of sub-continental lithospheric mantle, French Massif Central. *Geochim. Cosmochim. Acta* 71, 1290–1311.
- Wittig, N., Pearson, D.G., Baker, J.A., Duggen, S., Hoernle, K., 2010a. A major element, PGE and Re–Os isotope study of Middle Atlas (Morocco) peridotite xenoliths: evidence for coupled introduction of metasomatic sulphides and clinopyroxene. *Lithos* 115, 15–26.
- Wittig, N., Pearson, D.G., Duggen, S., Baker, J.A., Hoernle, K., 2010b. Tracing the metasomatic and magmatic evolution of continental mantle roots with Sr, Nd, Hf and Pb isotopes. *Geochim. Cosmochim. Acta* 74, 1417–1435.
- Wittig, N., Pearson, D.G., Webb, M., Ottley, C.J., Irvine, G.J., Kopylova, M.G., Jensen, S.M., Nowell, G.M., 2008a. Origin of cratonic lithospheric mantle roots: a geochemical study of peridotites from the North Atlantic Craton, West Greenland. *Earth Planet. Sci. Lett.* 274, 24–33.
- Wittig, N., Pearson, D.G., Webb, M., Ottley, C.J., Sand, K.K., Jensen, S.M., Nowell, G.M., 2008b. Evolution of the mantle root beneath the North Atlantic Craton. 9th International Kimberlite Conference, Extended Abstract No. 9IKC-A-00267, pp. 1–3.

**Formation of the North Atlantic Craton: Timing and mechanisms  
constrained from Re-Os isotope and PGE data of peridotite  
xenoliths from S.W. Greenland**

*N. Wittig<sup>1,\*</sup>, M. Webb<sup>1</sup>, D. G. Pearson<sup>1</sup>, C. W. Dale<sup>1</sup>,  
C. J. Ottley<sup>1</sup>, M. Hutchison<sup>2</sup>, S. M. Jensen<sup>2,3</sup> & A. Luguet<sup>1,4</sup>*

<sup>1</sup>Arthur Holmes Isotope Geology Laboratory, Department of Earth Sciences, Durham University, South Road, Durham, DH1 3LE, UK

<sup>2</sup>Geological Survey of Denmark and Greenland, Øster Voldgade 10, 1350 Copenhagen, K, DK

<sup>3</sup>Intex Resources ASA, Munkedamsveien 45A, PO 0250 Oslo, NO

<sup>4</sup>Mineralogisch-Petrologisches Institut, Universität Bonn, Poppelsdorfer Schloss, 53115 Bonn, GER

*Present address:*

*GeoZentrum Nordbayern*

*Endogene Geodynamik*

*Schlossgarten 5*

*D-91054 Erlangen*

*Germany*

*Tel: +49 9131 85 26065*

*Fax: +49 9131 85 29295*

*eMail: [wittig@geol.uni-erlangen.de](mailto:wittig@geol.uni-erlangen.de), [hobbes@steinlaus.me.uk](mailto:hobbes@steinlaus.me.uk)*

**Formation of the North Atlantic Craton: Timing and mechanisms constrained from Re-Os isotope and PGE data of peridotite xenoliths from S.W. Greenland**

**Os isotope model ages**

i. The equation for the calculation of  $T_{MA}$  Os model ages is as follows (equation 1)

$$OsT_{MA} = \frac{1}{\lambda} \ln \left( \frac{{}^{187}Os/{}^{188}Os_{sample} - {}^{187}Os/{}^{188}Os_{chondrite}}{{}^{187}Re/{}^{188}Os_{sample} - {}^{187}Re/{}^{188}Os_{chondrite}} + 1 \right) \quad \text{Equation 1}$$

using a  ${}^{187}Re$  decay constant ( $\lambda$ ) of  $1.666 \times 10^{-11}$  (Lindner et al., 1989). No correction for potentially metasomatic  ${}^{187}Re$  is made.

ii. The concept of Rhenium depletion ( $T_{RD}$ ) Os model ages is based on  $T_{MA}$  Os model ages, but assumes that all Re is of metasomatic origin. Therefore, these Os model ages are calculated with  $Re/Os = 0$  resulting in younger model ages relative to  $T_{MA}$  (equation 2).

$$OsT_{RD} = \frac{1}{\lambda} \ln \left( \frac{{}^{187}Os/{}^{188}Os_{sample} - {}^{187}Os/{}^{188}Os_{chondrite}}{+1} \right) \quad \text{Equation 2}$$

iii. The concept of  $T_{RD}^{erupt.}$  Os model ages is also based on  $T_{MA}$  Os model ages. It assumes that all Re is of metasomatic origin. In contrast to  $T_{RD}$  Os model ages it is calculated in 2 steps, prior to the time of magmatic sampling with  $Re/Os = 0$  and  $Re/Os$  as measured to correct for the radiogenic growth of Os since the time of volcanic eruption as stated below (equation 3),

$$OsT_{RD}^{erupt.} = \frac{1}{\lambda} \ln \left( \frac{{}^{187}Os/{}^{188}Os_{sample}^{initial} - {}^{187}Os/{}^{188}Os_{chondrite}^{initial}}{+1} \right) \quad \text{Equation 3}$$

whereby the initial  ${}^{187}Os/{}^{188}Os$  is calculated as (equation 4)

$${}^{187}Os/{}^{188}Os_{sample}^{initial} = \left( {}^{187}Os/{}^{188}Os_{measured} - {}^{187}Re/{}^{188}Os_{measured} \right) * (\exp[\lambda * t] - 1) \quad \text{Equation 4}$$

and denotes the Os isotope composition at the time of volcanic eruption, which was in the case of the North Atlantic Craton at 585 Ma (North) and 260 Ma (South).

***Formation of the North Atlantic Craton: Timing and mechanisms  
constrained from Re-Os isotope and PGE data of peridotite  
xenoliths from S.W. Greenland***

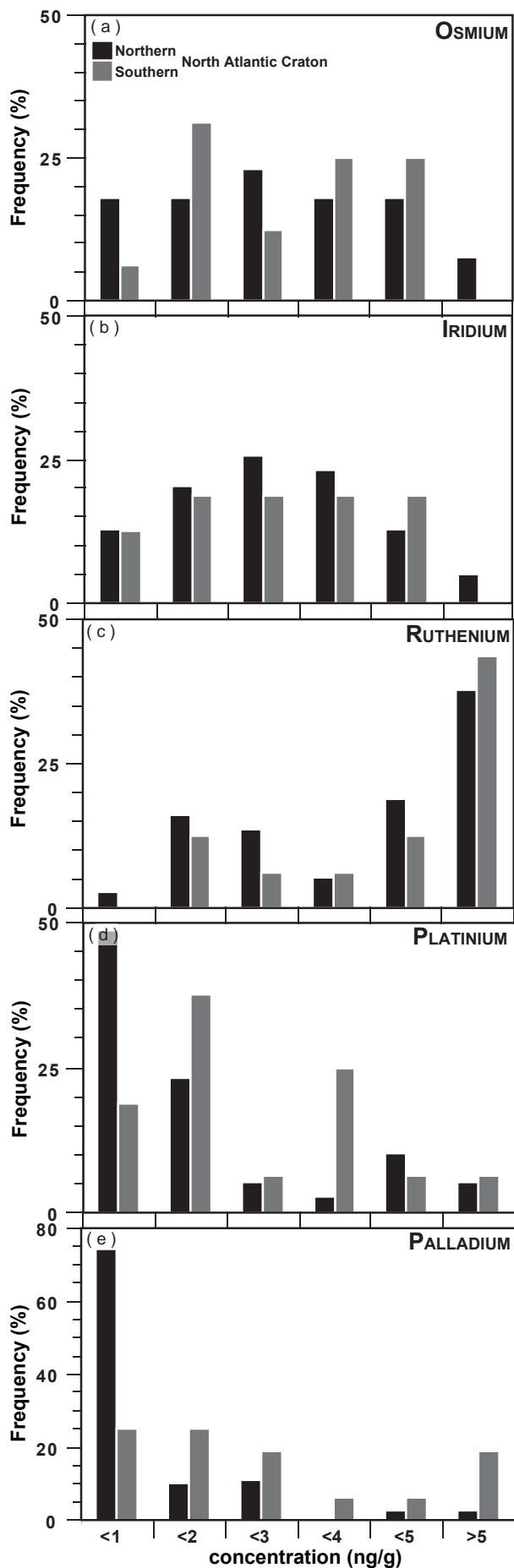
**Figures and Table**

Table A

Os isotope and PGE concentrations in parts per billion of chondrite and PRIMA used for data presentation and numerical modelling. Also given are 11 individual digestions (identified as batch numbers) of the Durham in-house peridotite standard GP13 and blank values that were derived during the course of this study.

	$^{187}\text{Os}/^{188}\text{Os}$	$2\delta$	$\gamma_{\text{Os}}$	Os	Ir	Ru	Pt	Pd	Re
<i>reference values</i>									
<b>chondrite</b>	0.12442	-	0	490	455	710	1010	550	30
<b>PRIMA</b>	-	-	-	3.4	3.6	5.0	7.1	3.9	0.28
<b>GP13<sup>a</sup></b>	0.1264	-	1.57	3.6	3.3	6.7	6.7	5.9	0.33
<i>Individual digestions of Durham in-house peridotite standard GP13 prepared during the course of this study and given per batch #</i>									
<b>p82-7</b>	0.12592 ± 8		1.21	3.76	3.47	6.55	6.4	5.8	0.33
<b>p88-7</b>	0.12589 ± 5		1.18	3.67	3.59	6.03	6.0	6.0	0.32
<b>p92-7</b>	0.12613 ± 10		1.38	3.92	4.41	6.69	8.0	8.4	0.33
<b>p93-7</b>	0.12628 ± 8		1.50	3.73	3.42	6.49	6.7	6.8	0.32
<b>p94-7</b>	0.12599 ± 6		1.27	3.68	3.55	n.d.	6.7	6.7	0.34
<b>p95-7</b>	0.12585 ± 5		1.16	3.88	3.83	6.66	8.0	5.7	0.33
<b>p97-7</b>	0.12583 ± 10		1.14	3.73	3.68	6.23	6.9	n.d.	0.35
<b>P110-6</b>	0.12620 ± 6		1.43	3.65	3.44	6.34	6.6	6.5	0.32
<b>P119-2</b>	n.d.	n.d.	n.d.	n.d.	3.42	6.66	7.6	6.9	0.32
<b>P121-7</b>	0.12632 ± 5		1.53	3.57	3.51	6.30	6.2	6.6	0.31
<b>P140-7</b>	0.12645 ± 9		1.63	4.22	3.69	7.18	7.6	8.1	0.34
<b>Average</b>	0.1261	-	1.31	3.8	3.6	6.5	7.0	6.7	0.33
<b>stdev</b>	0.0004	-	0.35	0.37	0.58	0.64	1.40	1.78	0.02
<b>RSD</b>	3	-	0.27	0.10	0.16	0.10	0.2	0.3	0.06
<i>Long-term reproducibility of the Durham in-house peridotite Standard GP13 (n = 33; 2004-2008)</i>									
<b>Average</b>	0.1261	-	1.39	3.77	3.58	6.85	6.9	6.4	0.32
<b>stdev</b>	0.0005	-	0.40	0.5	0.6	0.7	1.3	1.5	0.03
<b>RSD</b>	4	-	0.29	0.12	0.16	0.10	0.2	0.2	0.08
<i>Bulk partition coefficients used for PGE depletion models</i>									
<b>D</b>	-	-	-	1.E+05	1.E+05	4.E+03	9.E+03	1.E+03	-

**Notes:** All PGE except Ru were determined by sector field ICP-MS (Element2). Ru concentrations were acquired by quadrupole ICP-MS in collision cell mode (Xseries2). n.d. not determined. Relative standard deviation (RSD) is given as absolute value for PGE abundances and per mille for Os isotope data. Os isotope and PGE abundances of chondrite and PRIMA taken from Meisel et al. (1996) and Sun and McDonough (1995). <sup>a</sup>Literature value of GP13 and bulk partition coefficients taken from Pearson et al. (2004).



**Figure A**

Histogram of PGE concentrations shown in per cent (frequency) comparing I- (Os, Ir, Ru) and P-PGE (Pt, Pd) concentrations of the Northern (a, c) and Southern NAC (b, d). Note the strong mode of very low P-PGE concentrations of the Northern NAC (c) that is not present in the southern NAC (d).

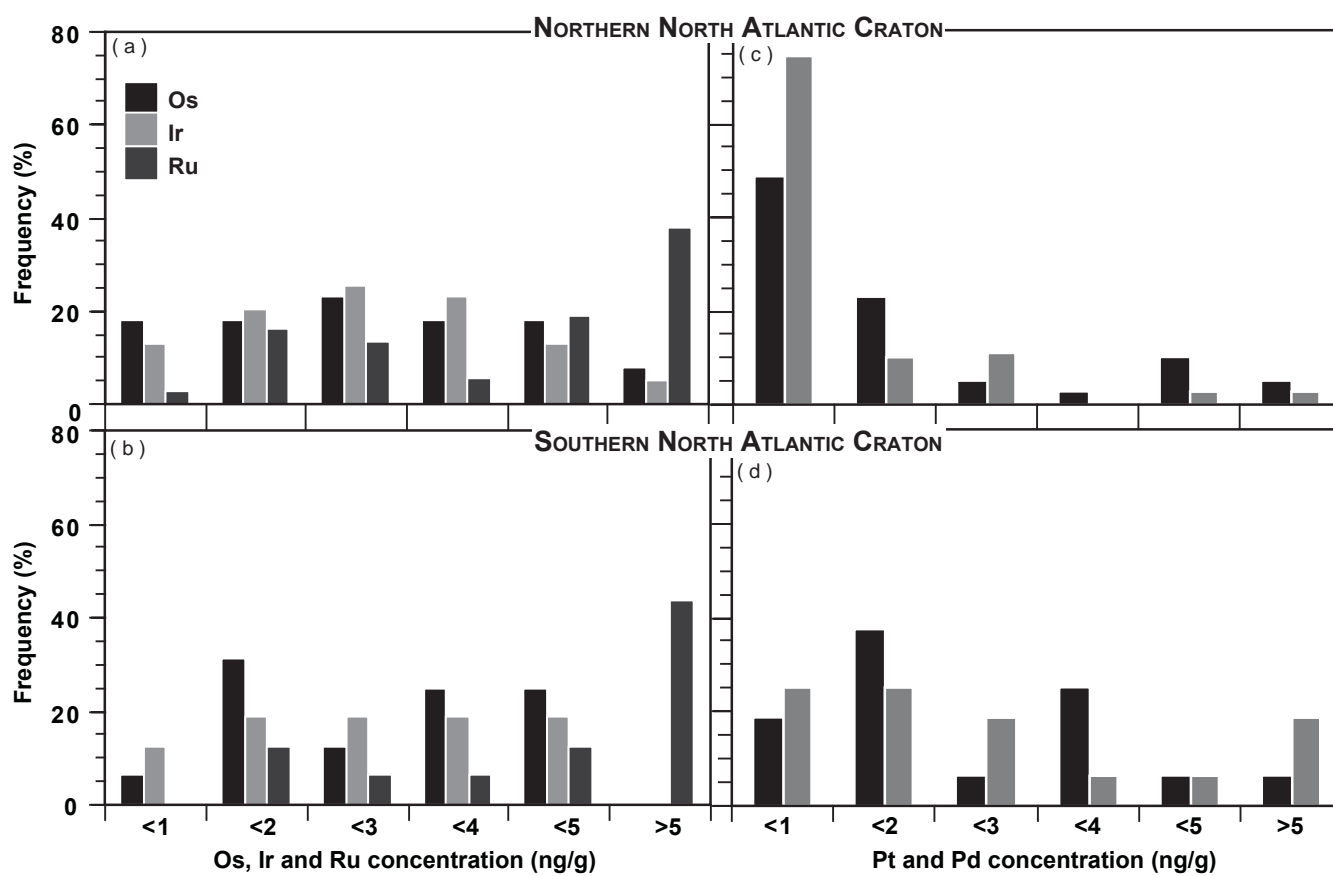


**Figure B**

Histogram of Os (a), Ir (b), Ru (c), Pt (d) and Pd (e) concentrations shown in per cent (frequency) comparing the Northern and Southern NAC. Note the strong mode of very low P-PGE concentrations of the Northern NAC (d, e) that is not present in the southern NAC (d).

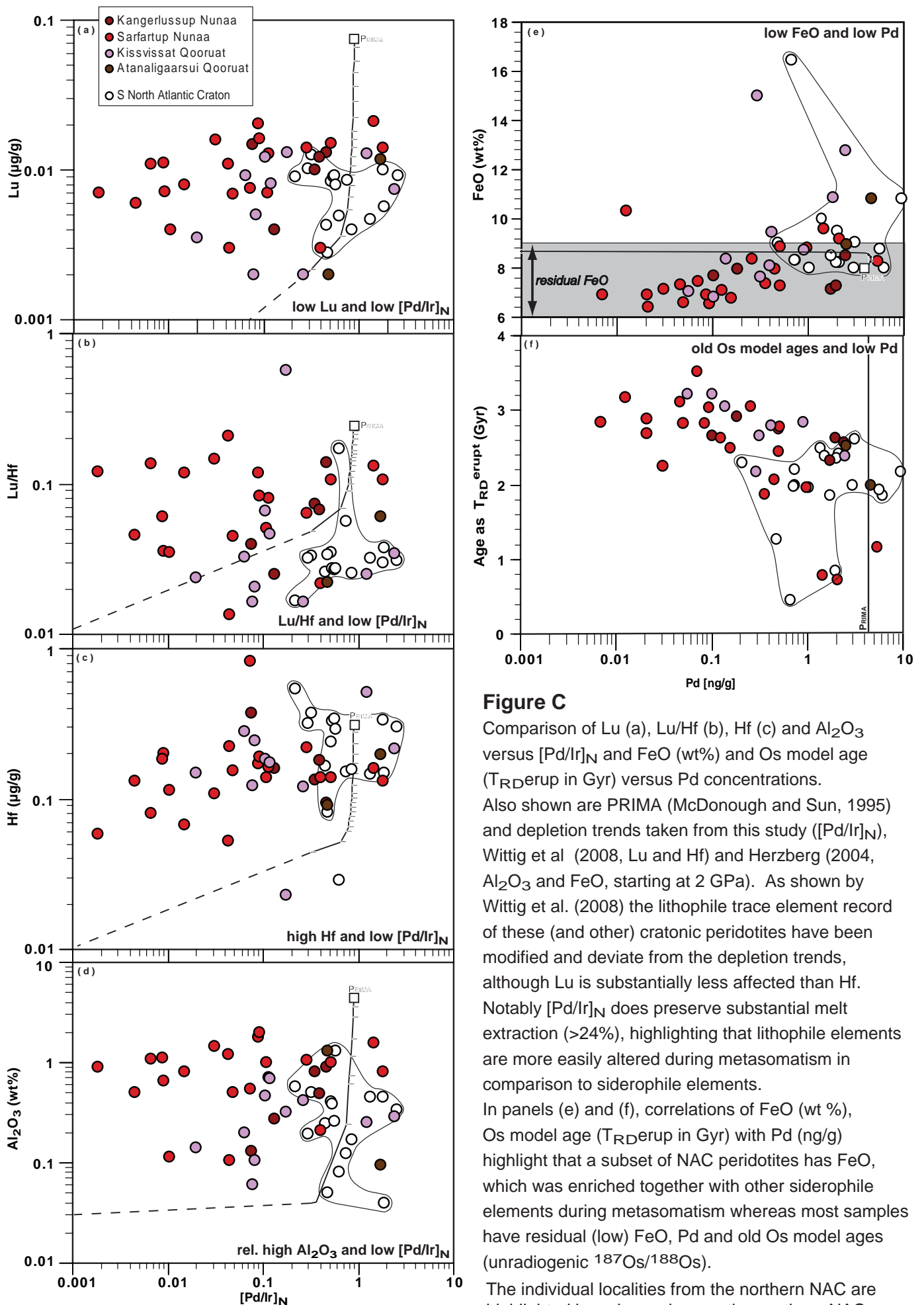


**Figure C**

Comparison of Lu (a), Lu/Hf (b), Hf (c) and  $\text{Al}_2\text{O}_3$  versus  $[Pd/Ir]_N$  and FeO (wt%) and Os model age ( $T_{RD\text{erupt}}$  in Gyr) versus Pd concentrations. Also shown are PRIMAs (McDonough and Sun, 1995) and depletion trends taken from this study ( $[Pd/Ir]_N$ , Wittig et al (2008, Lu and Hf) and Herzberg (2004,  $\text{Al}_2\text{O}_3$  and FeO, starting at 2 GPa). As shown by Wittig et al. (2008) the lithophile trace element record of these (and other) cratonic peridotites have been modified and deviate from the depletion trends, although Lu is substantially less affected than Hf. Notably  $[Pd/Ir]_N$  does preserve substantial melt extraction (>24%), highlighting that lithophile elements are more easily altered during metasomatism in comparison to siderophile elements. In panels (e) and (f), correlations of FeO (wt %), Os model age ( $T_{RD\text{erupt}}$  in Gyr) with Pd (ng/g) highlight that a subset of NAC peridotites has FeO, which was enriched together with other siderophile elements during metasomatism whereas most samples have residual (low) FeO, Pd and old Os model ages (unradiogenic  $^{187}\text{Os}/^{188}\text{Os}$ ).

The individual localities from the northern NAC are highlighted by colour, whereas the southern NAC samples are shown as open circles.

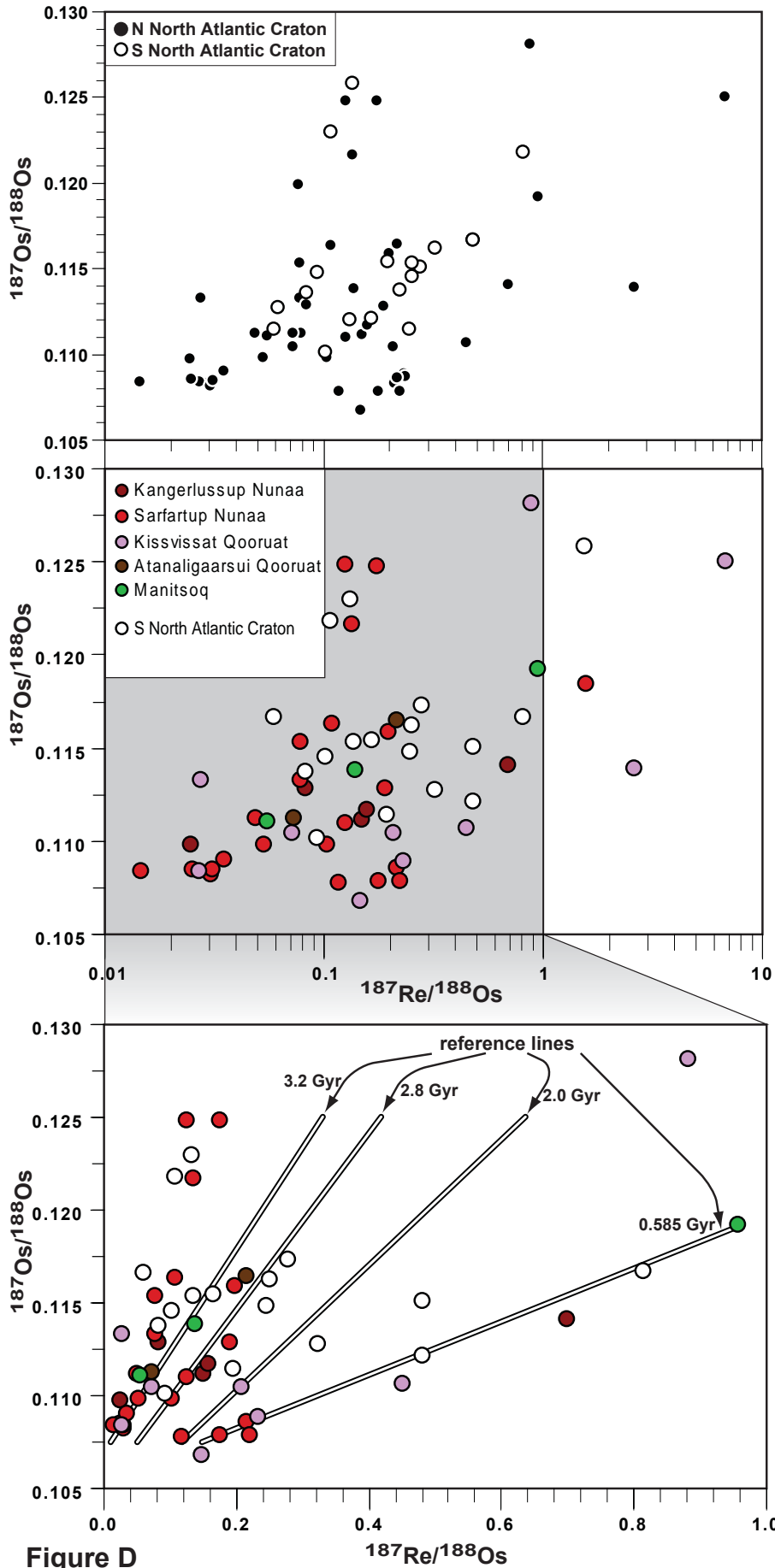


**Figure D**

$^{187}\text{Os}/^{188}\text{Os}$  versus  $^{187}\text{Re}/^{188}\text{Os}$  of whole-rock NAC peridotites. Panel (a) is identical as presented in the main manuscript whereas in panel (b) and (c) the individual localities from the Northern NAC are shown. Note the logarithmic x-axis ( $^{187}\text{Re}/^{188}\text{Os}$ ) in (a) and (b). The gray field in (b) is shown in (c) which features 3.2 Gyr, 2.8 Gyr, 2.0 Gyr and 0.585 Gyr reference lines. Note the general lack of isochronous correlations.

# $\gamma$ Os of Greenlandic peridotites

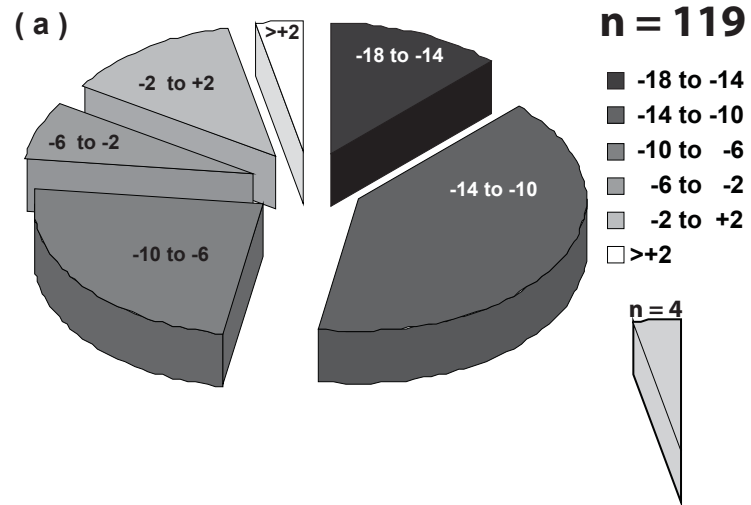
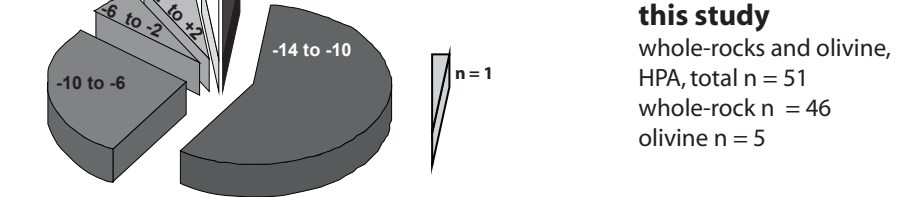


## Fig. E

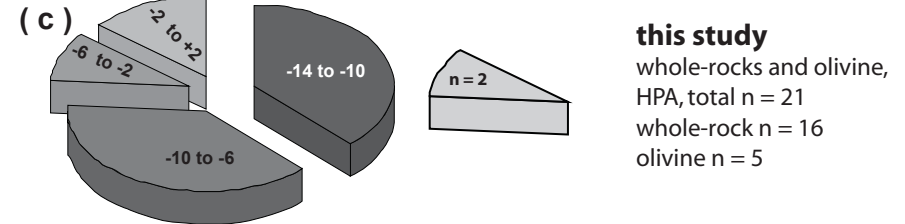
Compilation of Os isotope data (as  $\gamma$ Os) from Greenlandic peridotites. Panel (a) shows all data available from Greenland, comprising whole rock samples (n = 69), olivine (n = 29) and spinel (n = 21) data from the northern and southern NAC xenoliths (b, c), Disko Craton xenoliths (d), East Greenland xenoliths (e) and the orogenic peridotites from the central NAC (f).

Note the presence of very unradiogenic Os isotopes from all localities although no specific mode can be determined from the datasets from the Disko Craton and East Greenland. HPA and CT denote digestion methods using a high pressure asher and carius tubes.

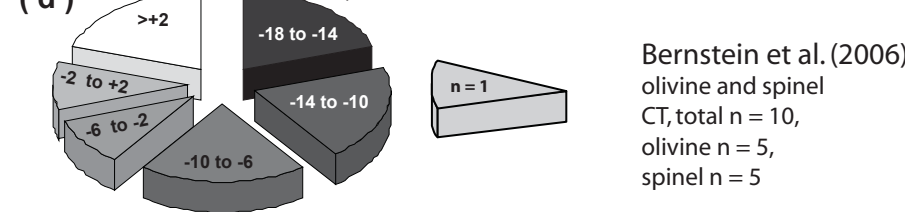
# $\gamma$ Os of northern NAC xenoliths



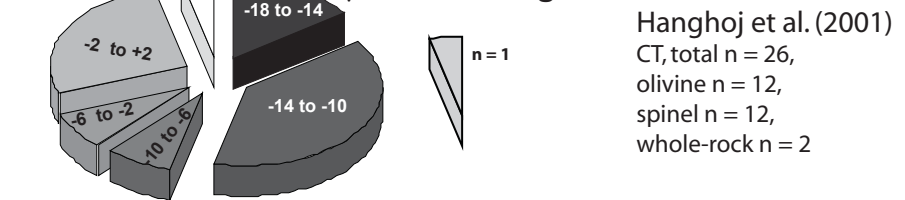
# $\gamma$ Os of southern NAC xenoliths



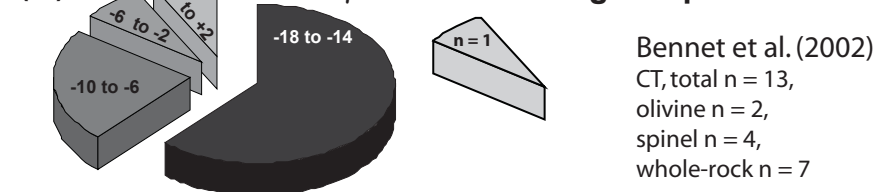
# $\gamma$ Os of Disko Craton xenoliths



# $\gamma$ Os of East Greenlandic xenoliths



# $\gamma$ Os of NAC orogenic peridotites



***Formation of the North Atlantic Craton: Timing and mechanisms constrained from Re-Os isotope and PGE data of peridotite xenoliths from S.W. Greenland***

**References**

- Bennett, V.C., Nutman, A.P. and Esat, T.M., 2002. Constraints on mantle evolution from  $^{187}\text{Os}/^{188}\text{Os}$  isotopic compositions of Archean ultramafic rocks from southern West Greenland (3.8 Ga) and Western Australia (3.46 Ga). *Geochimica et Cosmochimica Acta* 66, 2615-2630.
- Bernstein, S., Kelemen, P.B. and Hanghøj, K., 2006. Consistent olivine Mg# in cratonic mantle reflects Archean mantle melting to the exhaustion of orthopyroxene. *Geology* 35, 459-462.
- Hanghøj, K., Kelemen, P.B., Bernstein, S., Blustztajn, J. and Frei, R., 2001. Osmium isotopes in the Wiedemann Fjord mantle xenoliths: A unique record of cratonic mantle formation by melt depletion in the Archean. *Geochemistry, Geophysics, Geosystems* 2, 2000GC000085.
- Herzberg, C., 2004. Geodynamic information in peridotite petrology. *Journal of Petrology* 45, 2507-2530.
- Lindner, M., Leich, D.A., Russ, G.P., Bazan, J.M. and Borg, R.J., 1989. Direct determination of the half-life of  $^{187}\text{Re}$ . *Geochimica et Cosmochimica Acta* 53, 1597-1606.
- McDonough, W.F. and Sun, S.-s., 1995. The composition of the Earth. *Chemical Geology* 120, 223-253.
- Meisel, T., Walker, R.J. and Morgan, J.W., 1996. The osmium isotopic composition of the Earth's primitive upper mantle. *Nature* 383, 517-520.
- Pearson, D.G., Irvine, G.J., Ionov, D.A., Boyd, F.R. and Dreibus, G.E., 2004. Re-Os isotope systematics and platinum group element fractionation during mantle melt extraction: a study of massif and xenolith peridotite suites. *Chemical Geology* 208, 29-59.
- Walker, R.J., Shirey, S.B., Hanson, G.N., Rajamani, V. and Horan, M.F., 1989. Re-Os, Rb-Sr and O isotopic systematics in of the Kolar schist belt, Karnataka, India. *Geochimica et Cosmochimica Acta* 53, 3005-3013.
- Wittig, N. et al., 2008. Origin of cratonic lithospheric mantle roots: A geochemical study of peridotites from the North Atlantic Craton, West Greenland. *Earth and Planetary Science Letters* 274, 24-33.